Summer 2020

Synthesis of CdS/ZnS Core/Shell Semiconductor Nanoparticles

Austin Skyler Antle
Western Kentucky University, austin.antle922@topper.wku.edu

SYNTHESIS OF CdS/ZnS CORE/SHELL NANOPARTICLES

A Thesis
Presented to
The Faculty of the Department of Chemistry
Western Kentucky University
Bowling Green, Kentucky

In Partial Fulfillment
Of the Requirements for the Degree
Master of Science

By
Austin Skyler Antle

August 2020

SYNTHESIS OF CdS/ZnS CORE/SHELL NANOPARTICLES

Date Recommended 7/30/2020

Lawrence Hill Digitally signed by Lawrence Hill Date: 2020.07.30 16:07:46 -05'00'

Dr. Lawrence J. Hill, Director of Thesis

Matthew Nee Digitally signed by Matthew Nee Date: 2020.07.28 09:12:54 -05'00'

Dr. Matthew Nee

Bangbo Yan Digitally signed by Bangbo Yan Date: 2020.07.28 15:44:34 -05'00'

Dr. Bangbo Yan

8/7/2020

Associate Provost for Research and Graduate Education

ACKNOWLEDGMENTS

I would like to give a heartfelt thanks to Dr. Hill for guiding me through this graduate experience. Without him I would never have been able to push through as he has inspired me to be confident in my skills and knowledge. He also exposed me to a whole new area of chemistry that I had never thought of prior to becoming a graduate student. He has been able to alleviate so much stress and allow me to calmly think things through. My meeting and discussions with him will be remembered for years to come.

I would also like to thank my committee members Dr. Yan and Dr. Nee who have both helped in improving my thesis but also my seminar and writing skills. The evolution of my writing before their remarks and after truly astonished me as I never thought I could write such a scientific paper before.

A big acknowledgment must be given to Dr. Andersland. I have spent as much time working with him on the TEM as I have spent with everyone else combined though these past few years. Just as much time might have been spent just discussing research and life. He has truly been able to allow me to both learn scientifically but also think about life after my educational experience was over.

Perhaps no one has held my gradate career together as much as Haley who has been more help than I can say with words. I can’t name how many times I have had no idea what to do with a form or a submission and she has been able to get it all together even on almost no notice. Without her help I would not be here today.

My thanks go to Alicia as well who showed patience with me every time I came by with a question, even if it was the fifth time I was asking the same question. Not only did she encourage asking these, but she always had an answer for me even when she was busy. She was also the person who I could go to whenever there were issues in the teaching labs. Her advice on how to handle situations was invaluable.

Finally, I would like to thank Dr. Zhang who I have had the privilege of working with through every semester in both my graduate career but also my undergraduate. Whether he was my advisor, teacher, or oversaw the lab I was teaching I was able to learn so much from his vast knowledge. Without him I would not even be in the chemistry program, as he was the one who convinced me to give it another shot after I dropped out of the program as an undergraduate.

TABLE OF CONTENTS

Contents

Chapter

SYNTHESIS OF CdS/ZnS CORE/SHELL NANOPARTICLES

Austin Antle August 2020 55 Pages

Directed by: Lawrence Hill, Bangbo Yan, Matthew Nee

Department of Chemistry Western Kentucky University

Core/shell semiconductor nanoparticles are of great interest as photocatalysts due to their large surface area per volume and tunable band gaps. The synthesis of core/shell semiconductor nanoparticles has traditionally involved the use of binding ligands to ensure the particles do not aggregate. These binding ligands lower the surface area of the nanoparticles though, reducing their overall efficiency. Ionic liquids have been found to be capable of acting as both solvents and stabilizing agents for synthesis of catalysts with highly active surfaces. Our experiments focus on the synthesis of CdS/ZnS core/shell nanoparticles with the ionic liquid 1-butyl-3-methylimidazolium methyl sulfate, [BMIM][MeSO4], acting as both solvent and stabilizing agent. During synthesis we attempt to control the size of the synthesized particles and optimize the purification process to remove nanoparticles from [BMIM][MeSO4].

Chapter 1: Introduction

1.A- Introduction to nanoparticles as photocatalyst for solar energy

The search for cheap and clean renewable energy has taken on an even more prominent role in the scientific community due to the looming energy crisis the world faces. According to the US Energy Information Administration, fossil fuels make up 62% of the United States energy source as of 2019.[1] Nuclear power makes up 20%, with renewable energy sources only contributing 17.5%. Of this percentage wind and hydro power contribute 7% and 8%. Solar energy only makes up 2% of the energy production in the United States.

While working fine during sunny times, storage is necessary with solar energy in order to make it effective. This energy could be stored as electricity in batteries or as chemical energy in molecular hydrogen (the "hydrogen economy" coined by professor John Bockris in 1970). [2],[3] Both storage methods run into inherent problems. When stored as electricity the size of battery needed to supply a home is large, meaning it is expensive. This is becoming less of an issue with the advances in creating more efficient batteries. Some other answers to the storage problem are not only better batteries but large areas filled with many batteries known as battery farms. When stored as hydrogen the decision on whether to store as liquid or gas must be made. In both cases the energy density per volume is lower than hydrocarbon sources such as gasoline, equivalent to about a third the energy of gasoline. The enthalpy of combustion for gasoline is -5430kJ/mol. By dividing the enthalpy of combustion for gasoline (-5430kJ/mol) by the division of the molar mass (114g/mol) by the density (0.7g/mL), the energy density per volume can be calculated to be approximately 33kJ/mL. This can be repeated with hydrogen using its enthalpy (-

286kJ/mol) and dividing by the division of the molar mass (2g/mol) by the density (0.07g/mL), the energy density per volume can be calculated to be approximately 10kJ/mL.

$$H_2 + \frac{1}{2}O_2 \rightarrow H_2O \qquad \Delta_r = -286kJ$$

$$2C_8H_{18} + 25O_2 \rightarrow 18H_2O + 16CO_2 \qquad \Delta_r = -5430kJ$$

Water can be split into hydrogen and oxygen gas. This decomposition of water into hydrogen and oxygen is known as water splitting. For water to be decomposed it requires energy due to the positive enthalpy. This energy can be applied electrically (electrolysis) by passing a current through two electrodes in water. However, this electricity would most likely come from non-renewable sources. Alternatively, a photocatalyst can be employed to harvest photons of the appropriate energy for the water-splitting reaction. In 1972 photocatalysis was first reported as a method for the separation of water into hydrogen and oxygen gas.[4] The system used as seen in Figure 1.1 shows how light was used to power the process. When light hit the TiO_2 electrode an electrical current flowed from the Pt electrode to the TiO_2 electrode. This indicated oxidation (oxygen production) was occurring at the TiO_2 electrode and reduction (hydrogen production) was occurring at the Pt electrode.

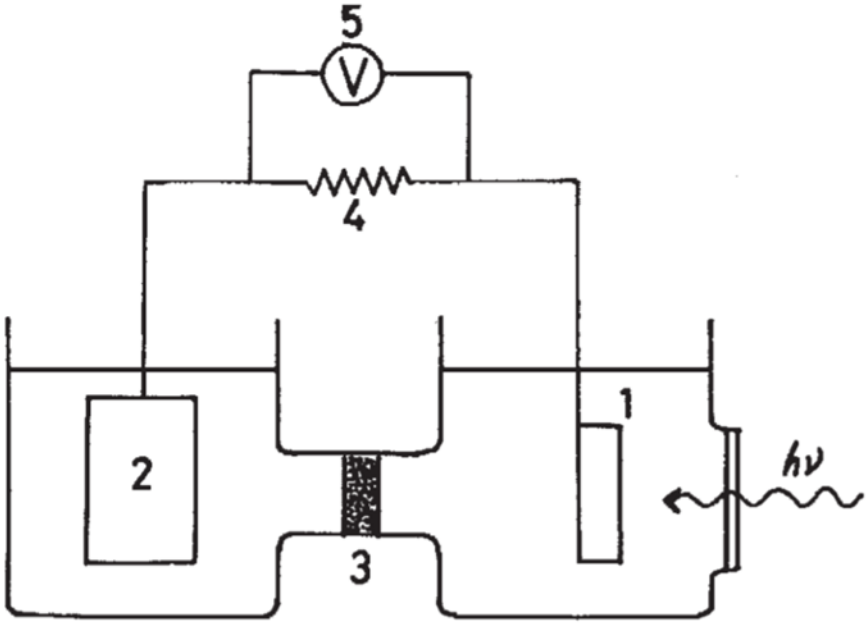

Figure 1.1: This diagram represents the electrochemical cell that was used to perform the first known water splitting using solar energy .Parts of the cell are labeled as follows, TiO_2 electrode (1), Pt electrode (2), Salt bridge (3), Resistance (4), Volt meter (5). (modified from reference 6)

The discovery of photocatalysis for water splitting led to a desire for a catalyst that could use solar energy to perform water splitting. Many different materials have been tested for their ability to catalyze this reaction; semiconductor nanoparticles (also known as quantum dots) with metal cocatalyst have been singled out by researchers though due to unique physical properties (surface area/volume) and electrical properties (tunable bandgap).[5]

1.B-Properties of semiconductor nanoparticles that are advantageous to photocatalysis

One of the most advantageous properties of nanoparticles is their ratio of surface area to volume. Figure 1.2 shows how the same volume of bulk material can be converted to a nanoparticle form and increase its surface area with the same amount of volume. This means that with more surface area there will be more surface locations for photocatalysis to occur. This leads to nanoparticles being a more cost effective and productive catalyst for water splitting than bulk materials.

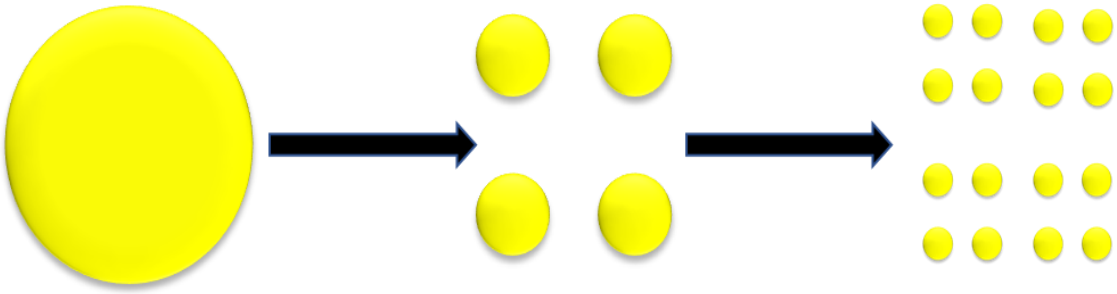

Figure 1.2: With the same volume of material the nanoparticles will have a higher surface area then the bulk material.

Perhaps the most beneficial property of semiconductor nanoparticles is their tunable bandgap. The optical properties of semiconductor nanoparticles are dependent on their size, meaning that by controlling the size of the nanoparticles the absorbance and emission of the particles can be controlled. Figure 1.3 shows, as semiconductor nanoparticles grow, their bandgap decreases leading to an absorbance and emission at lower energy wavelengths.

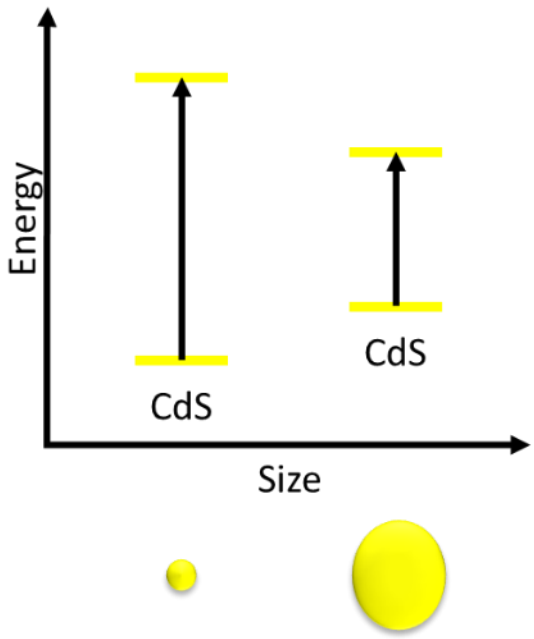

Figure 1.3: As semiconductor nanoparticles increase in size their bandgap decreases. This allows control over the absorption and emission of particles by controlling size.

1.C- Core/shell metal/semiconductor nanoparticles

A core/shell photocatalyst functions by accepting a photon from light. When this photon hits the photocatalyst a charge separation will occur as seen in Figure 1.4.[6] The negative charge that forms can then be used for hydrogen production (reduction reaction). The positive charge is used to convert the OH^- produced from the hydrogen formation into oxygen gas (oxidation reaction). The photocatalyst cannot easily accept another photon until both charges are removed.[7] However, it is also possible for the positive and negative charge to recombine without performing any catalysis. One method used to prevent charge recombination is to alter the morphology of the nanoparticles into nanorod structures. This provides a greater distance for the charges to be separated.

In order to replicate the photochemical electrode in Figure 1.1, semiconductor nanoparticles require a metal cocatalyst to perform the reduction part of the water splitting reaction. This metal cocatalyst not only facilitates the reduction reaction but aids in preventing charge recombination. As seen in Figure 1.5 the metal cocatalyst will isolate the negative charge. While the negative charge is isolated the positive charge can still freely move throughout the nanoparticle. In order to isolate the positive charge core/shell nanoparticles have been synthesized, thus creating a location for the positive charge to be isolated. Core/shell nanoparticles are nanoparticles formed by growing a second semiconductor layer around a previously synthesized semiconductor nanoparticle. By trapping the positive charge in the core and the negative charge in the metal cocatalyst, recombination of the charges can be delayed allowing more time for them to be used in catalysis.

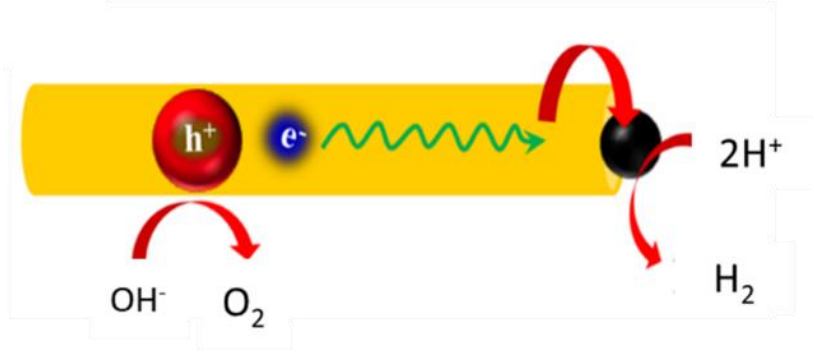

Figure 1.4: A photon from light causes a charge separation in the photocatalyst. The negative charge that forms from the separation will be used to split the water via hydrogen reduction. The positive charge will be used to convert OH^- into oxygen gas. (Modified from Ref.6)

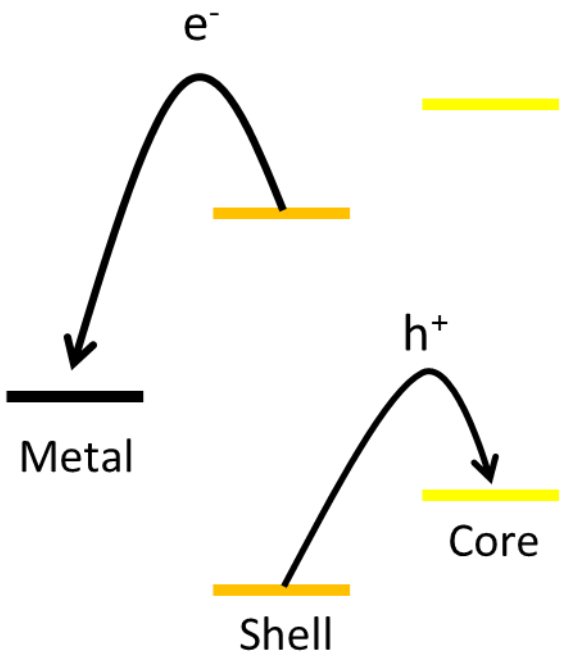

Figure 1.5: An energy diagram for Figure 4. Negative charge will be isolated in the metal cocatalyst. The positive charge will be isolated in the "core" of the nanoparticle.

The localization of the positive and negative charge, and subsequently the location of the oxidation and reduction reactions, has had the benefit of allowing researchers to test the rate of the individual half reactions. This individual testing has shown the removal of the positive charge localized in the "core" of the core/shell nanoparticle to be the rate-limiting step of the water splitting reaction. Due to the difficulty in accepting a photon for more charge separation before both the positive and negative charges are removed, this slow removal of the positive charge limits the rate of the overall reaction.

1.D: Synthesis of semiconductor nanoparticles

When synthesizing nanoparticles, a bottom-up approach is typically taken over a top-down method. This means that instead of turning bulk material into nanoparticles, the

particles are instead synthesized from molecular precursors. Whenever nanoparticles are synthesized there is a major issue that needs to be overcome pertaining to their size. While the small size of the particles is part of what makes them excellent photocatalyst, it also makes them aggregate together. Once the particles reach the nanometer size, surface energy becomes high enough between the particles to begin causing aggregation. Once the particles aggregate together, they lose all benefits gained from synthesizing them at the nanoscale size. To prevent this aggregation during synthesis in organic solvents (such as 1-octadecene) an insulating ligand is added to the reaction. This insulating ligand such as oleic acid seen in Figure 1.6 will attach to the surface of the nanoparticles and prevent them from aggregating together.

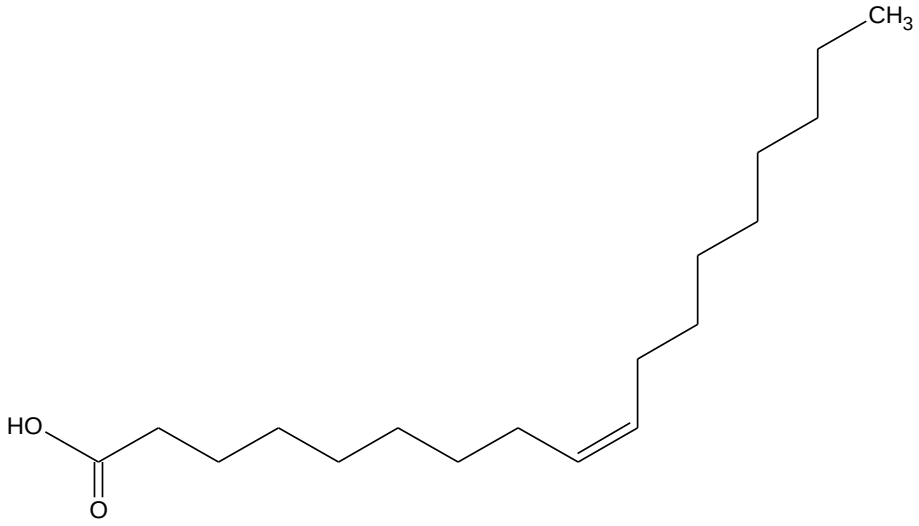

Figure 1.6: Ligands are used to prevent nanoparticle aggregation. Here the structure for oleic acid can be seen. Oleic acid is a possible insulating ligand that can be used to prevent nanoparticle aggregation.

These insulating ligands also have drawbacks to being used. As stated earlier photocatalysis for hydrogen production is a surface level chemistry, meaning that the more

surface area the better. Yet the insulating ligands themselves cause a loss in surface area when attaching to the particles. These ligands can also cause issues when implementing these particles into industrial devises due to causing a buildup of insulating material. As the particles are used to coat a surface, there is also a buildup of the insulating ligands.

1.E- Ionic liquids for the synthesis of semiconductor nanoparticles

Ionic liquids are salts that are in the liquid phase below 100°C and typically contain a bulky organic cation paired with either an organic or inorganic anion.[8–10] These ionic liquids have been shown to help promote synthesis of nanoparticles and are theorized to stabilize nanoparticles synthesized in them due to unique structural properties.[11]

The properties of ionic liquids vary greatly depending on the cations and anions that compose the ionic liquid but possess some intrinsic properties present in all ionic liquids that indicate they are an excellent medium for the development of efficient photocatalytic nanoparticles. Ionic liquids have a surface tension that is higher than organic solvents and lower than water.[12] This intermediate surface tension allows for an optimal level of nucleation while being low enough to prevent Ostwald ripening. This can lead to a uniform size of nanoparticle throughout.

What truly separates ionic liquids as solvents for nanoparticle synthesis is their inherent structure they have, even in the liquid phase. This structure is formed from a mixture of electrostatic, hydrogen bonding (between the imidazolium or cation and the anion), and van-der-Waals interactions.[13] These forces combine to create an organized three-dimensional structure in the liquid phase. When nanoparticles are added to the ionic liquid these hydrogen bonds are disrupted or broken apart as seen in Figure 1.7. Once broken apart multiple polar and non-polar regions are formed within the ionic liquid. These

structured regions help organize the nanoparticles. Once the nanoparticles are integrated into the system of the ionic liquid it is theorized that they are stabilized by ion layers that form around the nanoparticles from the cations and anions that make up the ionic liquid as seen in Figure 1.7.[14]

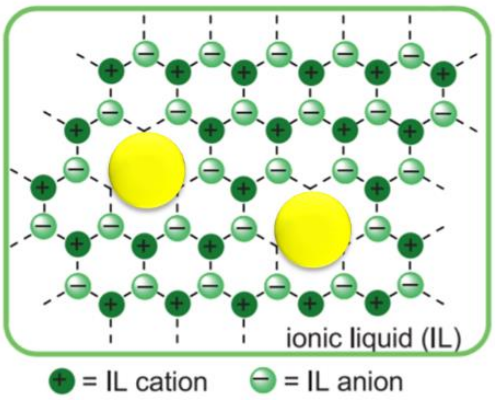

Figure 1.7: Nanoparticles are theorized to be electrosterically (electrostatic and steric) stabilized when grown or placed in ionic liquids due to the creation of polar and non-polar regions upon the introduction of nanoparticles to the system. This causes an ion layer to form around the nanoparticles that work to stabilize the particles. (Modified from Ref.14)

Core/shell semiconductor nanoparticles synthesized in ionic liquids have been found to have increased catalytic activity when compared to nanoparticles synthesized with insulating ligands.[15] These nanoparticles synthesized in ionic liquids can generate nearly twice the amount of hydrogen via water splitting than the same particles synthesized with ligands.

Our research is focused on the synthesis of a complete metal/semiconductor hybrid catalyst using ionic liquids to compare performance with insulated catalysts. Our system consists of a core/shell CdS/ZnS nanoparticle with attached Pt cocatalyst stabilized by the

ionic liquid used for the synthesis. By performing the full synthesis in ionic liquids, we aim to form catalysts with little aggregation and relatively high surface area per unit volume. We believe this will aid in the rate limiting step of removing the positive charge from the nanoparticles and lead to a more efficient photocatalyst.

Chapter 2: CdS/ZnS core/shell nanoparticles capped with oleic acid and oleylamine

Our research began by synthesizing CdS/ZnS core/shell particles using 1-octadecene as our solvent. The particles would be insulated with oleic acid (our ligand of choice) as seen in Figure 2.1. These particles would then be characterized in order to determine particle size and concentration. This step would allow us to obtain experience with the processes used to synthesize core/shell particles for future experimentation. These particles could also be used as a basis to compare with nanoparticles synthesized using our new method.

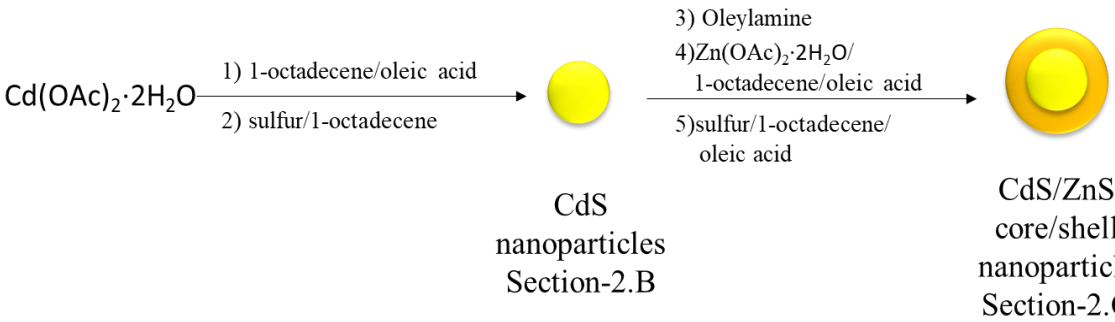

Figure 2.1: One-pot synthesis of CdS/ZnS core/shell nanoparticles described this chapter. CdS nanoparticles were synthesized by injection of a sulfur solution into hot octadecene containing cadmium acetate and oleic acid. Zinc shells were then grown on these particles by alternating addition of $Zn(OAc)_2 \cdot 2H_2O$ and sulfur in the presence of oleylamine.

2.A: Materials and methods

2.A.1: Materials

Acetone, 1-octadecene, methanol, toluene, hexanes, oleylamine, ethanol, cadmium acetate dihydrate ($Cd(OAc)_2 \cdot 2H_2O$), cadmium oxide (CdO), sulfur powder, zinc acetate dihydrate ($Zn(OAc)2 \cdot 2H_2O$), oleic acid, and thioacetamide were purchased from Sigma Aldrich and used directly with no further purification.

2.A.2: UV-vis spectroscopy procedure

UV-vis spectra were obtained using a UV-2600 UV-VIS Spectrophotometer by Shimadzu. A 0.5mL quartz cuvette was used to hold our samples. Samples were scanned over a wavelength range of 300nm to 800nm. Spectrophotometer was set on its slowest setting, scanning at 1nm increments. System was blanked by scanning our cuvette with the solvent our particles were dispersed in. Data was saved as a .txt file to be used in Microsoft excel. Data was then used to create scatter plots.

2.A.3: Fluorimetry procedure

Fluorimetry was performed on a Shimadzu RF-5301 PC spectrofluorometric fluorometer. A 5mL quartz cuvette optically polished on four sides was used to hold samples during testing. Samples were diluted in solvent before use. Solvents used were tested prior to scanning our samples to ensure they had no emission reading. If a reading was observed this would be subsequently subtracted from tested samples data. Samples were scanned at 0.5nm increments at 100 scans per minute. Samples were scanned using an excitation wavelength of 390nm with an observed range of 400nm to 800nm. The data for each sample was transferred individually to an excel file. Once the data for each sample

was on an excel file the data would be modified in order to construct a scatter plot of the spectra.

2.A.4: Transmission Electron Microscopy (TEM) imaging procedure

For TEM imaging a JEOL 1400Plus transmission electron microscope was used to observe synthesized particles. Imaging was performed with a voltage setting of 100kv. Images ranged from 100x magnification to 250000x magnification. The filament used was LaB_6. Copper grids (200 mesh) were coated with a thin carbon film and used to hold our samples during imaging by placing in the sample holder. The copper grids were coated with carbon in lab using carbon-coated mica which was prepared from raw mica and carbon rods. The fixtures which hold the carbon were from Ladd Research Industries: 30170 – carbon rod evaporation unit 30180 - carbon evaporation shield. The carbon was from EMS Cat #70200, sharpened to about 4 mm with a #12040 carbon rod sharpener from E. Fullam. The glass shield was coated with "Bell Shine" from Ladd #30099. Our vacuum evaporator was built by Torr International, model number: TH#-2KW-UPGRD-EB1P operated initially in the 10-6 torr range vacuum range, and at about 40 Amps. The mica was fixed into a clean petri dish which was then placed on a 50mL beaker making it approximately 5-10cm from the graphite rod. The mica was coated using an indirect coating method using a quarter affixed directly above the mica so that the coating would be consistent and reduce the overall thickness of the coat. Water was then used to separate the mica from the carbon by placing water droplets onto a PELCO PTFE immunostaining pad (product #10526-1), purchased from Ted Pella Inc. The carbon-coated mica was cut into small squares, slightly larger than a copper TEM grid, and placed carbon side up into the water droplet at an angle from the side of the droplet to quickly remove the carbon layer. Due to the mica being

hydrophilic in nature and carbon being hydrophobic, the mica would sink into the water droplet while the thin layer of carbon would remain at the top of the droplet. The floating carbon film was then lifted onto a copper TEM grid, ensuring that the carbon film covered as much of the grid as possible. The copper grids were washed in hydrochloric acid prior to carbon coating to facilitate breaking through the surface of the droplet. The grid would be placed in a tray to dry by a pair of tweezers. Using a small slip of paper made removing the grid from the tweezers easier as the grid would otherwise stick to the tweezers.

2.A.5: Centrifugation procedure

Samples were centrifuged using a Thermo Scientific Sorvall ST 8 having a radius of 12cm in 50mL polypropylene centrifuge tubes from VWR (max rcf 17,000 g). Samples were centrifuged at 7000rpm at ten-minute increments until particles crashed out.

2.B-Cadmium Sulfide Nanoparticle Growth

Our first objective was the synthesis of CdS nanoparticles in 1-octadecene that were insulated with oleic acid. This synthesis can be seen in Figure 2.2. Once synthesized we characterized our synthesized CdS nanoparticles using UV-vis, fluorimetry, and TEM.

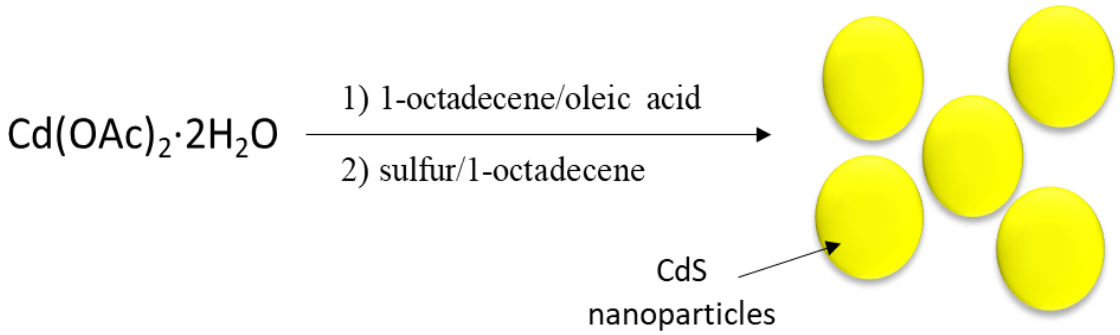

Figure 2.2: $Cd(OAc)_2 \cdot 2H_2O$ was dissolved in 1-octadecene and oleic acid at 260°C and sulfur solution was added via syringe. This allowed our CdS nanoparticles to form. Once formed, by maintaining temperature our particles could grow to our desired size.

2.B.1: Procedure for CdS nanoparticle synthesis

Sulfur stock solution was made by adding elemental sulfur (0.032g, 1mmol) to a 20mL vial. Afterwards a rubber septum was placed on the vial and an inert environment was induced by vacuuming out atmosphere and replacing with argon. Once under an inert environment, 1-octadecene (10 mL) was added via syringe to the vial. The vial was swirled to mix up the solution and then placed on a heating mantle set to 180°C and heated until sulfur was dissolved. Stock solution was stored in a dark environment at room temperature until needed for future synthesis. When used for subsequent reactions the solution is reheated to 180°C until sulfur is dissolved again.

$Cd(OAc)_2 \cdot 2H_2O$ (0.046g, 0.2mmol) was added to a three-neck round-bottom flask and an inert environment was induced by three alternating vacuum/argon cycles. 1-octadecene (10mL) and oleic acid (0.25mL, 0.8mmol) were transferred to the flask via syringe. The solution was then heated to 260°C to allow the $Cd(OAc)_2 \cdot 2H_2O$ to dissolve, indicated by a color change from brown to clear and colorless. Temperature of solution was monitored by an internal temperature probe, ensuring accurate temperature measurement. After it was confirmed that the $Cd(OAc)_2 \cdot 2H_2O$ fully dissolved, we proceeded to form the CdS nanoparticles. 1mL (0.1mmol) of the sulfur stock solution was added to the flask via syringe and allowed to cool to 240°C. The solution sat at 240°C for 15 minutes to allow particles to fully grow.

At this point, the as-synthesized CdS nanoparticle dispersion can be used directly for the addition of ZnS shells by the SILAR method (described in section 2.C) or the

particles can be purified for characterization (described in the remaining portion of section 2.B below).

Purification to remove our particles from the 1-octadecene, cadmium acetate, cadmium oleate, and oleic acid was performed by centrifugation. The solution was cooled to around room temperature. The crude product was divided between two 50mL centrifuge tubes. The flask was washed with 10mL methanol followed by 30mL hexanes and divided up between the two centrifuge tubes to ensure all particles were removed from the flask. Centrifuge tubes were filled to 50mL mark with acetone. Centrifugation was performed at 6000rpm for ten minutes on each sample of nanoparticles. The supernatant was decanted, and the pellets were dispersed in hexanes and transferred to a 20mL vial. One drop of the hexanes dispersion was used to cast a sample onto a TEM grid via pipette. A 1mL sample was transferred into a 2mL vial to be used for UV-vis and fluorimetry. Addition of acetone to the centrifugation procedure was instrumental as without, no pellets ever formed, while pellets formed after one centrifugation in the presence of acetone.

2.B.2: UV-Vis Spectroscopy

Approximately 0.3mL of the CdS nanoparticle dispersion in hexanes was transferred to a quartz cuvette with two optically polished sides. The UV-vis data were collected on the slowest setting possible to get as smooth a spectrum as possible. We obtained a UV-vis spectrum of our samples showing a shoulder at approximately 422 nm; the low-energy peak absorbance was estimated from this spectrum as seen in Figure 2.3. This absorbance value is what was used to estimate the diameter and concentration of our particles as described below.

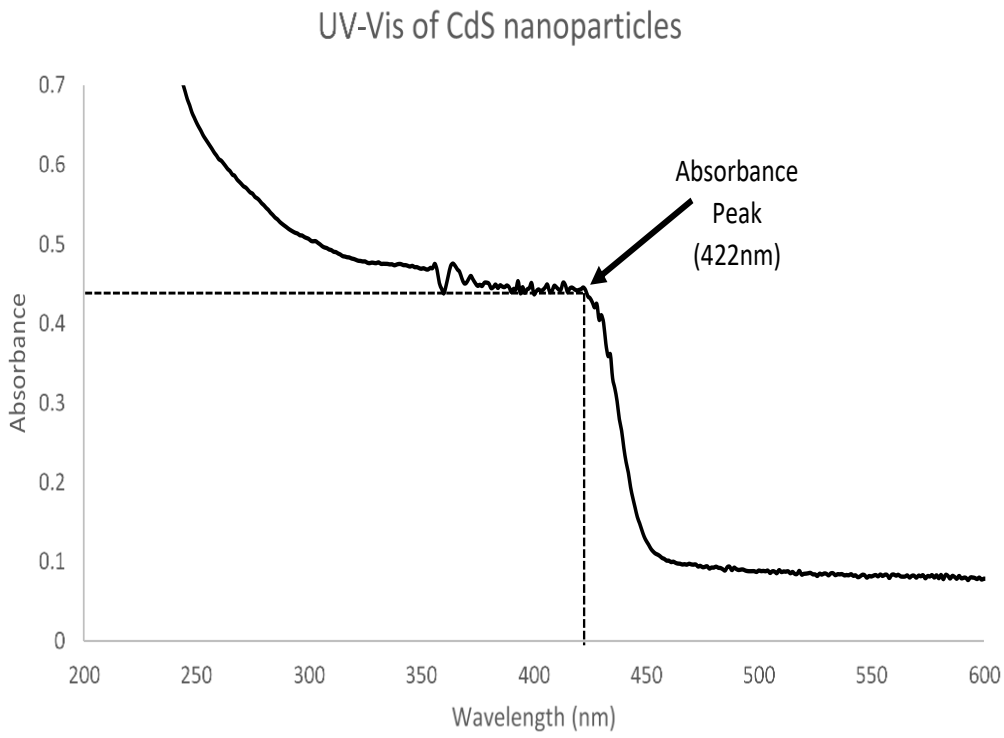

Figure 2.3: UV-Vis spectroscopy was performed on our synthesized nanoparticles to help confirm they were CdS. The absorbance peak obtained matches the known location of CdS nanoparticle absorbance peaks.[16]

CdS nanoparticle diameter (D)

$$D=(-6.6521\times10^{-8})\lambda^3+(1.9557\times10^{-4})\lambda^2+(9.2352\times10^{-2})\lambda+(13.29) \quad (1)$$

Extinction coefficient (ε)

$$\varepsilon = (21536)(D)^{2.3} \quad (2)$$

Absorbance (A)

$$A = (\varepsilon)*\text{length of cuvette}(L)*\text{concentration}(C) \quad (3)$$

Peng and coworkers reported an empirical correlation between the low-energy peak absorbance wavelength (λ) and nanoparticle diameter (D, equation 1), as well as a correlation between nanoparticle diameter and extinction coefficient (ε, equation 2).[16] In

order to determine the location of the peak shown in figure 2.3, we assumed that the shoulder of our spectrum was the right side of a symmetrical curve which has a gaussian-like distribution. The estimated peak was used as our absorbance peak for Peng's equation. This method was done for determining our absorbance peak due to our spectra showing a shoulder instead of a defined peak. Using this we were able to determine our peak as seen in Figure 2.3 being at 422nm. This wavelength value was used to estimate the diameter of our particles by equation 1. Using our calculated diameter, we could estimate the extinction coefficient for our particles using equation 2. With the extinction coefficient and absorbance value from our peak we could estimate the concentration of our particles in solution using equation 3.

2.B.3: TEM Imaging

TEM imaging was then performed on our particles to obtain the image seen in Figure 2.4. Average particle diameter equaled 1.8nm with a standard deviation of 0.4nm when 100 particles were sized. These sizes were obtained using imageJ software.[17] Initial imaging of particles was difficult due to an aging filament in our TEM. This aging filament went unnoticed due to most imaging done at our institution being at lower magnifications. A new filament was obtained for our microscope that allowed clear images at high magnification for our particles.

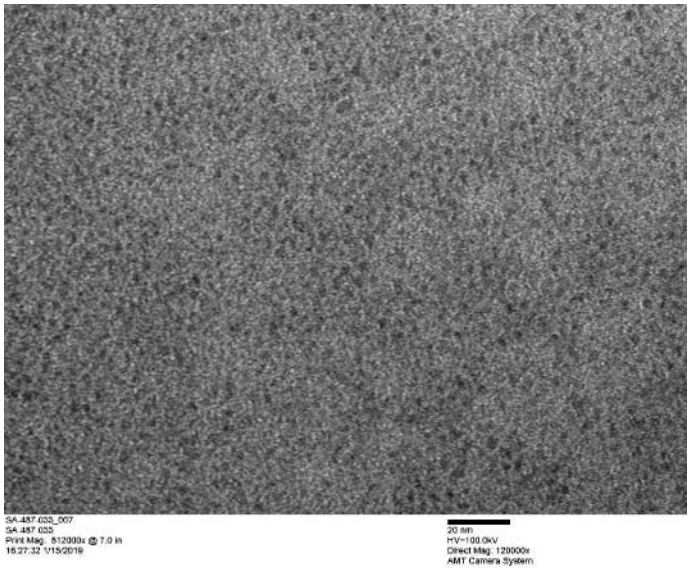

Figure 2.4: TEM imaging was performed on our CdS particles. Upon looking at our images we could clearly see numerous particles that had been formed with a spherical morphology. Scale bar of image represents 20nm. Average size of particles in the image above equaled 1.84nm ± 0.4nm. 100 particles were measured for average size calculation.

Upon characterization with UV-vis and TEM we could conclude with strong confidence that we had synthesized CdS nanoparticles. The lowest energy peak of CdS is known to be between 350nm and 450nm.[16] While our peak was not a perfect absorbance peak but instead a shoulder, this has been reported by others.[18] The weak contrast in TEM imaging was also consistent with CdS nanoparticles.

2.B.4: Tracking of CdS particle growth over time

We then followed the nanoparticle growth reaction to estimate the size of our nanoparticles at certain time points for use in subsequent experiments growing ZnS shells. In order to monitor the reaction process, the CdS nanoparticles were synthesized following the same procedure shown in section 2.B.1. After the sulfur stock was injected, 0.7mL

samples were taken at time points and absorbance peaks were observed as seen in Figure 2.5. These peaks could be used to determine the size of the particles using equation 1 as seen in Table 2.1. We determined that the CdS particles grew (using the equation-1) until they reached their maximum size at 10 mins. After 10 mins the particles remain the same size. After looking at this data we decided to allow our CdS particles to grow for 15mins to allow the particles to reach their maximum size

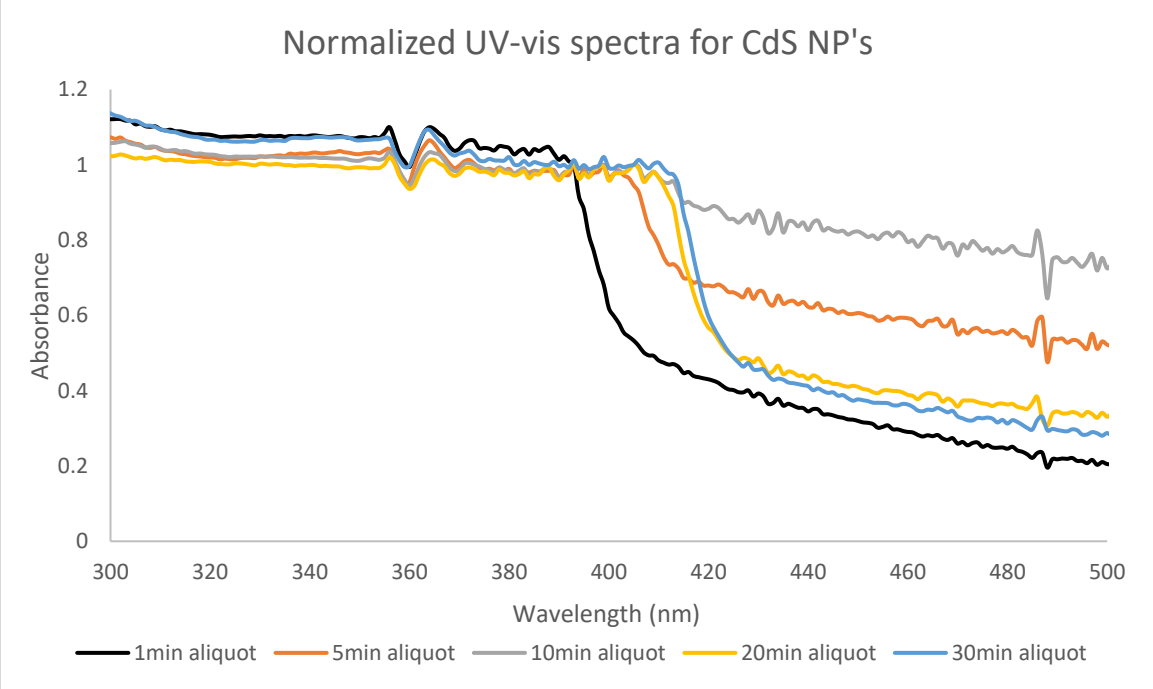

Figure 2.5: UV-vis spectroscopy was used to find the absorbance peak for different time points of growth for the CdS cores. These peaks can be used in calculations to estimate the size of the nanoparticles at a time point.

Table 2.1: The wavelength of the absorbance peak is used to calculate the diameter of the particles. These can be seen in the above table for the five time points we checked for size. These values correspond to the peaks in Figure 2.5

Time Point	Wavelength value of peak (nm)	Diameter (nm)
1min	393	3.2
5min	400	3.4
10min	410	3.7
20min	410	3.7
30min	410	3.7

2.B.5: Fluorimetry

Figure 2.6 shows the fluorimetry reading obtained from CdS nanoparticles. Our UV-vis spectra showed a peak at 422nm; therefore, we expected an emission peak to appear at a slightly higher wavelength. The peak emission intensity was weak. A small peak can be seen at about 410nm and a small broad peak at about 550nm. This signals that our CdS nanoparticles do not have strong emission and that the excited electrons relax preferentially through non-radiative pathways.

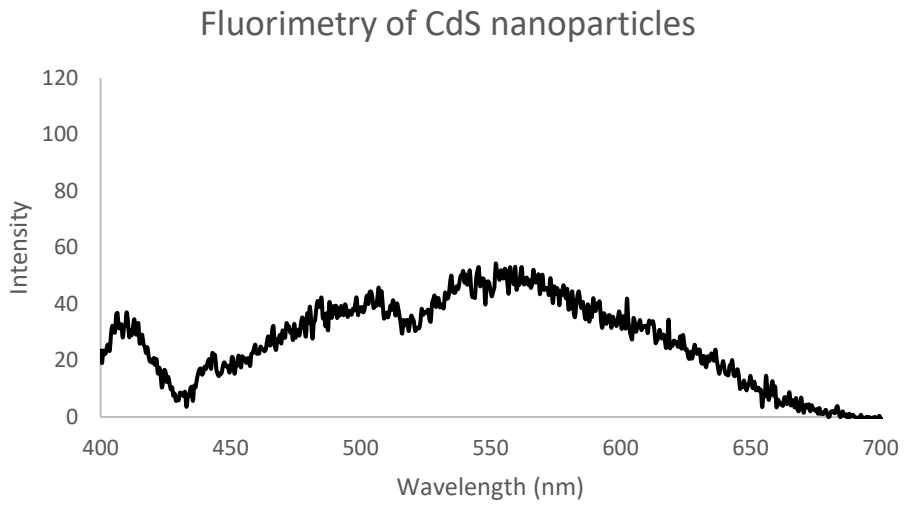

Figure 2.6: Fluorimetry was performed on the CdS nanoparticles. Excitation wavelength was set at 390nm

2.C: Zinc sulfide shell growth vis SILAR method

Once CdS nanoparticles had been synthesized and characterized we could begin growing ZnS shells. This process is illustrated in Figure 2.7.

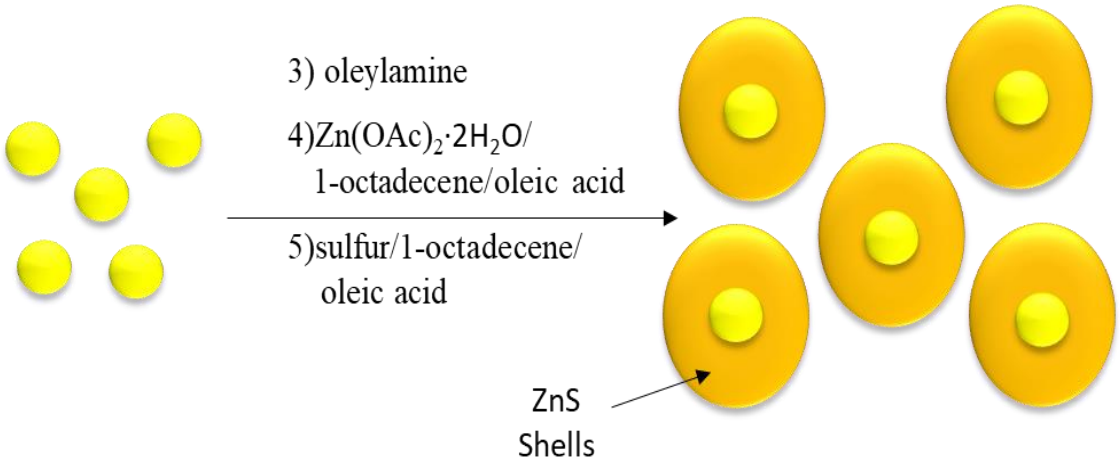

Figure 2.7: Our CdS nanoparticles from 2.B.1 are used as the "core" for core/shell growth. Zinc and sulfur solutions are injected in subsequent injections to grow ZnS layers. Repeating injection will grow additional layers increasing the overall size of our ZnS shell.

2.C.1: Procedure for ZnS shell growth

A zinc stock solution was prepared by transferring zinc acetate dihydrate (0.2195g, 1mmol) to a 20mL vial, before sealing with a rubber septum. An inert environment was induced by vacuuming out atmosphere and replacing with argon before oleic acid (3mL, 0.009mol) and 1-octadecene (7mL) were added via syringe. The solution was placed on a heating mantle set to 150° until the zinc acetate was fully dissolved (indicated by turning clear and colorless).

A dispersion of CdS nanoparticles in octadecene and oleic acid was prepared as described in section 2.B.1, and the size and concentration of the nanoparticles in the dispersion was determined by UV-vis spectroscopy. The size and concentration of CdS nanoparticles were used to determine the amounts of zinc and sulfur stock solutions to use at each injection (Table 2.2, details of this calculation are shown in section 2.C.1). Then, 2mL of oleylamine was injected into the three neck round bottom flask at 50°C and was immediately heated to 220°C. 31µL of zinc stock solution was injected into the flask at temp and allowed to sit for five minutes. Immediately after five minutes 31µL of sulfur stock solution was injected into the flask via syringe and the temp was increased to 240°C. The zinc and sulfur were allowed to react for twenty minutes before cooling the solution back to 220°C and transferring a 0.3mL sample to a 1mL vial for characterization.

Table 2.2: This table was created quickly from our calculation sheet to know exactly how much of our stock solutions to inject for every layer. Knowing the amounts quickly was imperative in order to ensure our particles were grown evenly and efficiently

layer number	μmol of Zn/S needed	μL of Zn/S needed
0	0	0
1	3.1	31
2	4	40
3	5.5	55
4	6.7	67
5	8.5	85
6	10	100

This process was repeated with the increasing amounts of stock solution used from Table 2.2 until six cycles were completed, with samples taken after each heating and cooling cycle. The crude product, after samples were taken, was divided between two 50mL centrifuge tubes. Flask was washed with 10mL methanol followed by 30mL of hexanes and divided up between the two centrifuge tubes to ensure all particles were removed from the flask. Centrifuge tubes were filled to 50mL mark with acetone. The samples were centrifuged at 6000rpm for ten minutes. The supernatant was decanted, and the pellets were dispersed in hexanes and transferred to a 20mL vial. A 1ml sample was transferred into a 2ml vial for characterization. TEM samples were prepared for each sample by transferring a single drop onto a carbon coated TEM grid, that was on a paper

towel, via pipette. The remaining amount of each sample was used for UV-vis and fluorimetry.

2.C.2: Calculating amounts of zinc and sulfur needed to grow multiple ZnS layers

For the growth of the ZnS shell we decided to use the SILAR method (Successive Ionic Layer Adsorption and Reaction) to synthesize and grow our shells.[19] This method involves the growth of the shell in layers via multiple subsequent injections of the zinc and sulfur stock solutions. In order to start we needed to know the size of the CdS nanoparticles. This is determined by using the absorption peak from UV-vis. The low-energy peak wavelength and the absorbance value at this wavelength were used to calculate the diameter and concentration of our particles in solution. This is done as described in section 2.B.2 using equations 1-3.[16] The wavelength from the absorbance peak is used to estimate the diameter of the CdS nanoparticles. The diameter is then used to estimate the extinction coefficient. Finally, the extinction coefficient is used with the absorbance value from the low-energy absorbance peak to estimate the concentration of CdS particles in solution prior to addition of ZnS.

The calculation for the amount of ZnS required to form a single monolayer on a CdS nanoparticle can be thought of as a simple subtraction problem.[19] This is illustrated in Figure 2.8. From the previous experiments we determined how to calculate the diameter of the CdS nanoparticles synthesized by using their absorbance peak. From the diameter we can determine the radius of the particles. The radius is then used to calculate the volume of the CdS nanoparticles. The volume of the CdS/ZnS core/shell particle can be determined by using the same volume equation for a sphere but adding 0.31nm to the radius. This is due to each layer of ZnS being 0.31nm in thickness. The volume of the CdS nanoparticle

can then be subtracted from the CdS/ZnS core/shell particle to get the volume of the ZnS shell. The amount of zinc and sulfur needed can be calculated by taking the volume of the ZnS shell and multiplying by the density of ZnS ($4.1 \times 10^6 g/m^3$). The number of moles this equates to is determined by dividing the mass of the ZnS shell by the molecular weight of ZnS (97.474 g/mol). All these calculations are for just one CdS/ZnS particle, therefore the moles needed for one particle can be multiplied by the concentration of particles in solution calculated using equation 3. This process can be repeated for each layer, using the previously synthesized ZnS shell as the starting volume. These calculations were inserted into a excel file to create a calculation sheet to quickly give us all the amounts needed for every shell we grow.

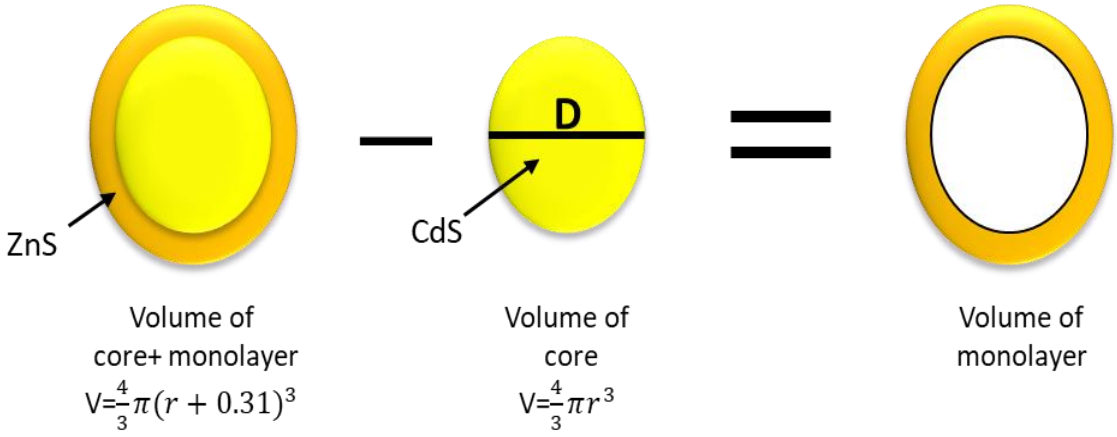

Figure 2.8: The calculations used determine the amount of zinc and sulfur for needed to form each shell by subtracting the volume of the core from the volume of the core and the first layer. This is repeated for every shell layer grown.

Figure 2.9 shows the absorbance peak obtained from UV-vis spectroscopy of CdS nanoparticles grown for 15 minutes. The diameter and concentration of the CdS particles

were determined as described in section 2.B.2, and the concentration was multiplied by the reaction volume to give us the total number of particles of CdS in solution. The total number of CdS nanoparticles was used to determine the amounts of zinc and sulfur needed to grow our six layers as seen in Table 2.2.

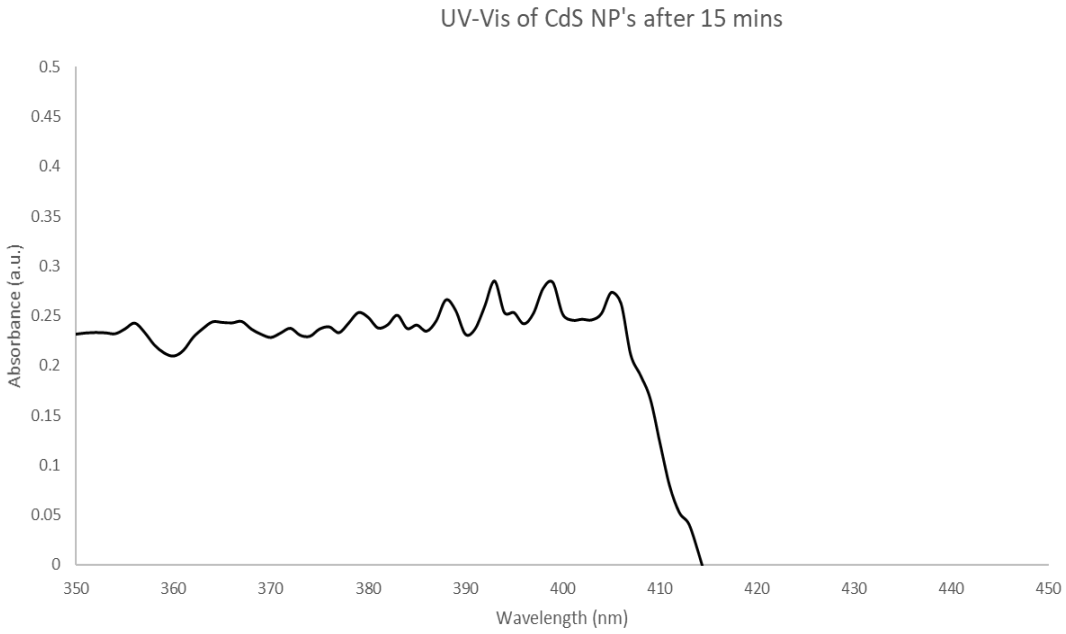

Figure 2.9: This absorbance peak from CdS nanoparticles taken after 15mins gave us the absorbance and wavelength values we needed in order to calculate the diameter of our particles synthesized. This would then be used in order to calculate amounts needed for SILAR.

2.C.3: UV-vis characterization of ZnS shell growth

We obtained our UV-vis spectra showing the absorbance of our CdS/ZnS core/shell particles as seen in Figure 2.10. Upon observing the spectra, the absorbance peak can be observed shifting to a lower energy state upon each addition of ZnS. As observed when

checking the growth of the CdS nanoparticles, the movement of the absorbance peak to higher wavelengths corresponds to the particle growing.

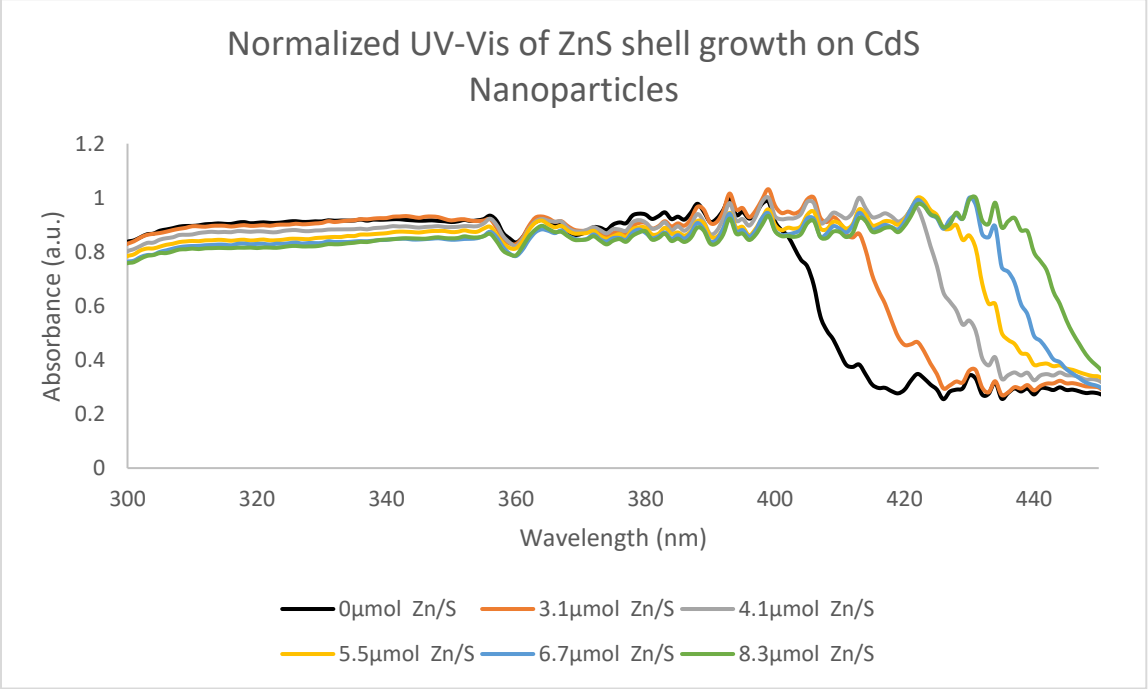

Figure 2.10: UV-vis spectroscopy was performed on each sample taken from the SILAR shell growth. The absorbance peak moves downfield (red shifting) with each subsequent layer growth. This shows that the particle is growing continuously larger.

2.C.4: Fluorimetry characterization of ZnS shell growth

We also took our samples, still in the vial, and put them under a UV lamp. Using this we could see the red shift of the particles with our naked eyes. This was an easy and quick indicator that our particles sizes had changed with the growth of the shell. The initial CdS particles can be seen as light green color in Figure 2.11. As the shell was grown, they began to shift to a yellow color. By the time the final shell layer was grown the color had shifted to a darker orange color. These colors are due to the CdS/ZnS core shell particles

absorbing the UV-light and then emitting the color. This emission can be recorded and plotted by fluorimetry.

Figure 2.11: CdS nanoparticle dispersion (left) and CdS/ZnS core/shell nanoparticle dispersions with increasing shell thickness (from left to right) viewed under a UV lamp. The emission colors could be seen changing from the green to orange. This allowed us to see the red shift with our own eyes

An excitation wavelength of 390nm was used for our emission readings. Fluorimetry characterization can indicate if the shell is growing around our particles. This is due to fluorimetry reading the emission, which is when the electron that is excited in the bandgap relaxes and falls an energy level.

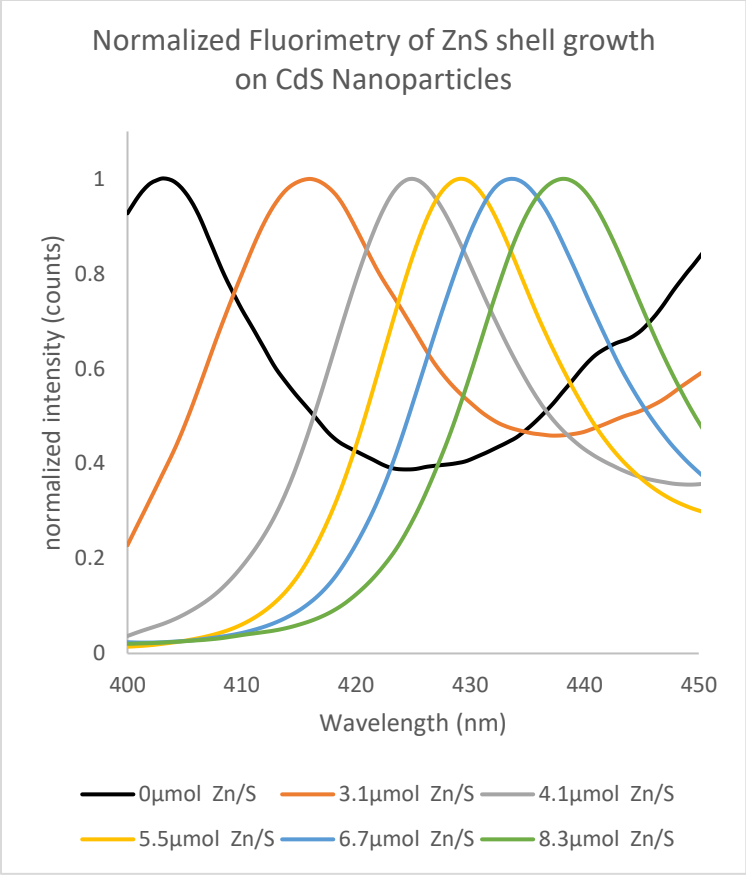

Figure 2.12: Fluorimetry was performed on the samples taken from our SILAR shell growth. The emission peak moves downfield with each layer added, just like the UV-vis. This further helps confirm that our particles are growing. Excitation wavelength was set to 390nm.

Figure 2.13a,b,c shows the effect of mixing of the band edge energy levels of CdS and ZnS. [20] The resulting mixed band edges are closer in energy than the original CdS band edges, resulting in a lower energy band gap (indicated by a red line in figure 2.13). While the CdS bandgap remains the same size during growth of the ZnS shell, the ZnS bandgap decreases in size as more zinc and sulfur are added to the reaction mixture. The smaller

ZnS bandgap results in a smaller mixed bandgap with CdS, which accounts for the decreasing bandgap (red shifting peak) of our CdS/ZnS core/shell particles as they grow.

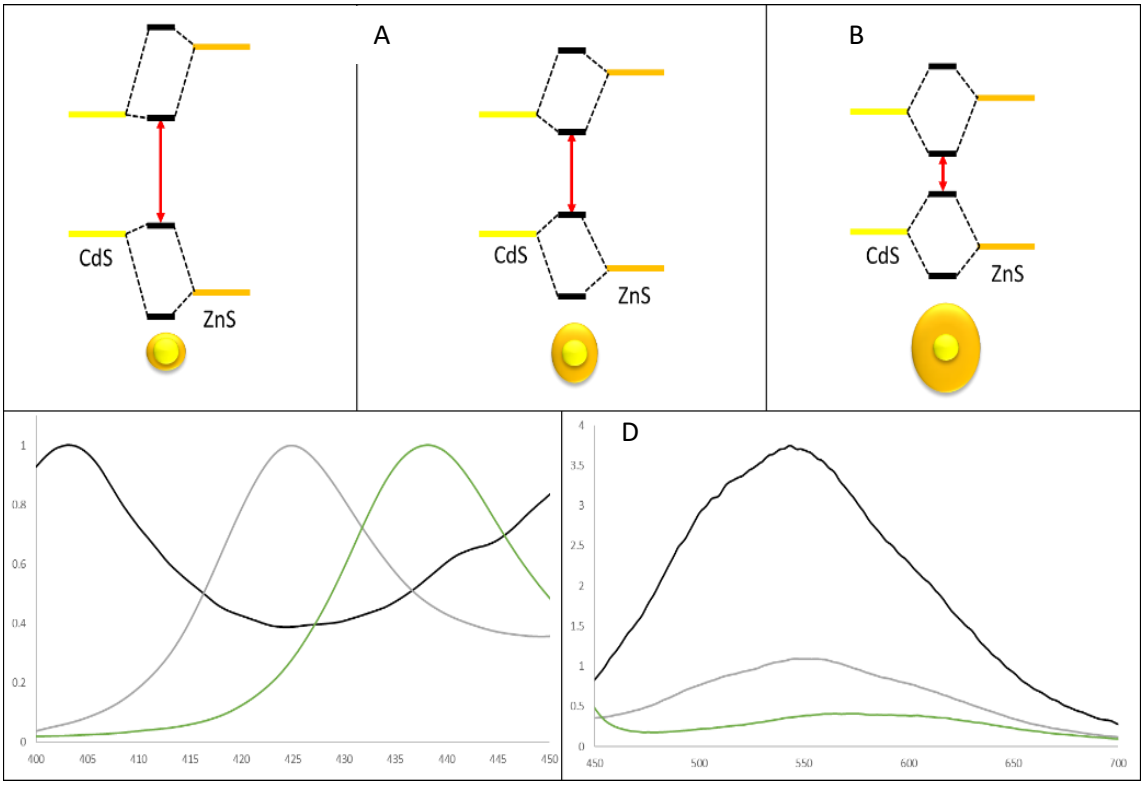

Figure 2.13: Images A,B, and C show the mixed bands that form from the conduction and valence bands of the CdS and ZnS. Image-D shows an example of the fluorimetry red shifting. Image-E shows a broad peak that red shifts as the ZnS shell is grown, but also decreases in intensity as the shell is grown.

In Figure 2.14 a second peak can be observed at 580nm. Previous studies have shown that this peak can be attributed to the effects of surface-state traps.[21] The surface trap states are due to surface cadmium on the CdS nanoparticle that has a vacancy and no ligand attached. This allows the cadmium to act as an electron trap. This matches the data we see, as the peak shrinks in size as the shell is grown. This explains why the broad second

peak decreases in intensity in comparison to the first peak with every layer of the ZnS shell grown. As the shell is grown there is less of the CdS core exposed, leading to less of a chance for a trap state to occur.

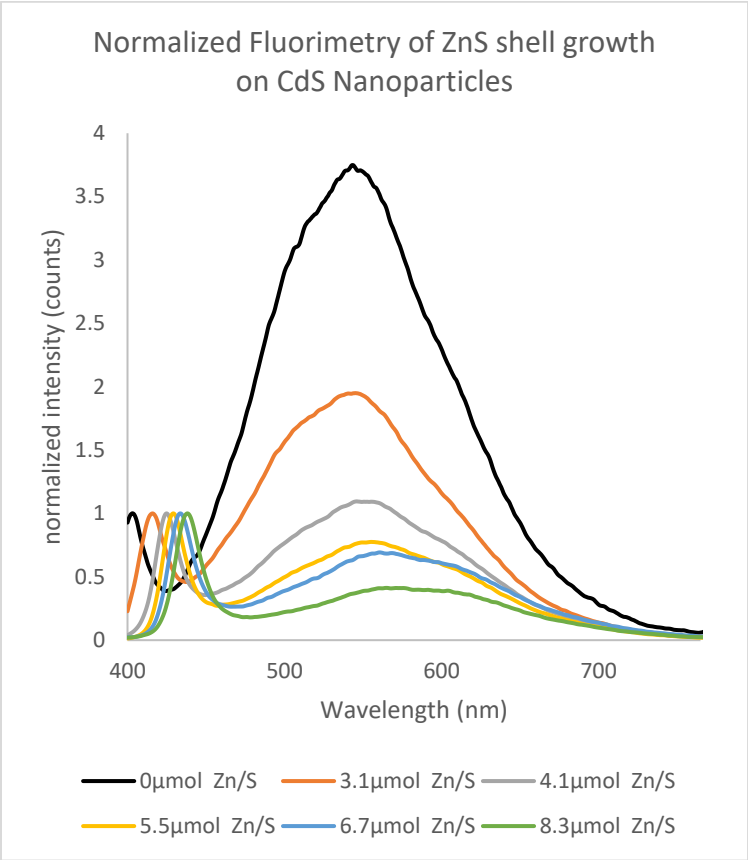

Figure 2.14: A second peak could be seen in our fluorimetry readings. After investigation we noticed a trend that the second peak got smaller in comparison to the first peak as our shells were grown. We concluded that this peak was from surface trap states.

2.C.5: TEM characterization of ZnS shell growth

TEM imaging was performed on all samples taken to observe their size and morphology, and two of these images are shown in Figure 2.15. The particles from image-A, after adding one equivalent of ZnS, are smaller than particles from image-B, after adding

six equivalents of ZnS. Upon sizing, the particles from Figure 2.15a had average diameters of d=1.58nm ± 0.26nm (n=100). Upon sizing image-B we found the average diameter to be d=3.17nm ± 0.47nm (n=100). The overall sizing distributions can be seen in Figure 2.16 below.

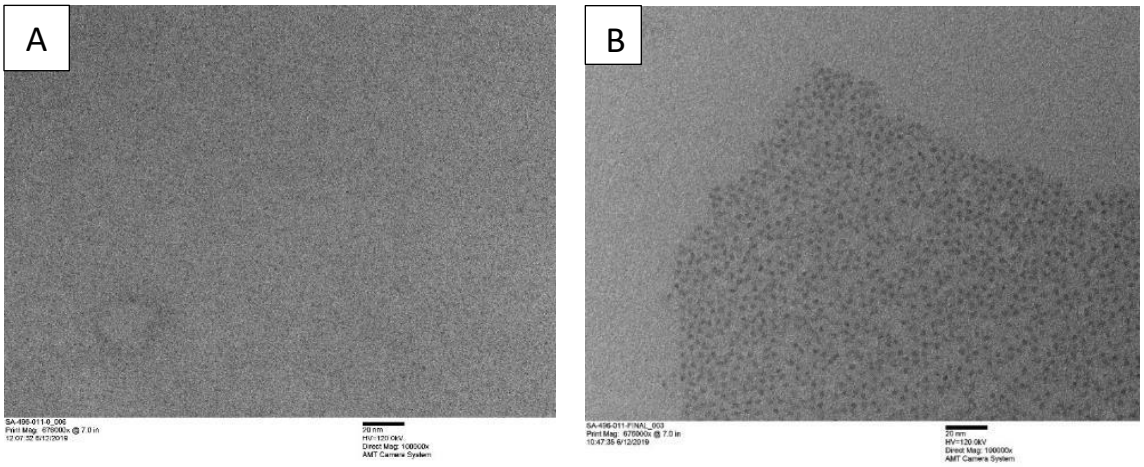

Figure 2.15: TEM images obtained after adding one equivalent of ZnS (A) and after adding six equivalents of ZnS (B). Both images are at 100000x magnification with 20 nm scale bars.

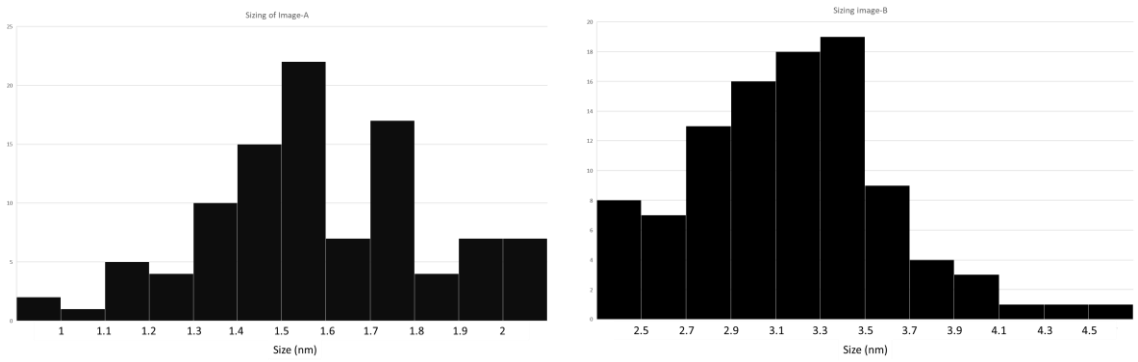

Figure 2.16: Histograms were made for the sizing of both image-A and image-B from Figure 18.

Chapter 3: Synthesis of CdS/ZnS core/shell nanoparticles [BMIM][$MeSO_4$]

Once CdS/ZnS core/shell nanoparticles had been successfully synthesized in 1-octadecene and characterized we began experimenting with the same synthesis in [BMIM][$MeSO_4$] as seen in Figure 3.1.

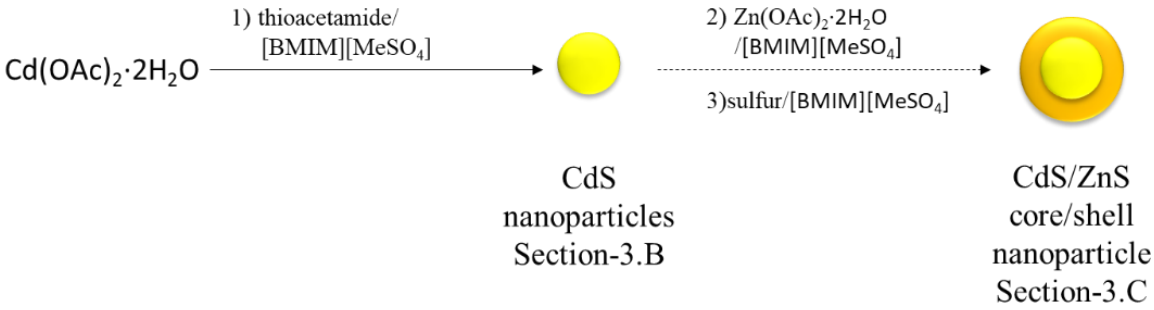

Figure 3.1: Reaction scheme for synthesis of CdS/ZnS core/shell nanoparticles [BMIM][$MeSO_4$].

3.A: Materials and methods

3.A.1: Materials

Acetone, 1-octadecene, methanol, toluene, hexanes, oleylamine, ethanol, cadmium acetate dihydrate ($Cd(OAc)_2 \cdot 2H_2O$), cadmium oxide (CdO), sulfur powder, zinc acetate dihydrate ($Zn(OAc)_2 \cdot 2H_2O$), oleic acid, and thioacetamide were purchased from Sigma Aldrich and used directly with no further purification. 1-butyl-3methylimidazolium methyl sulfate ([BMIM][$MeSO_4$]) was purchased from Sigma Aldrich and transferred from its purchased bottle into a smaller bottle in a glove box with an inert environment to ensure the majority of the sample remained uncontaminated with moisture, due to [BMIM][$MeSO_4$] being hygroscopic.

3.A.2: UV-vis spectroscopy procedure

UV-vis spectra were obtained using UV-2600 UV-VIS Spectrophotometers by Shimadzu. Samples were scanned at both the slowest setting and medium setting depending on if particles were observed to be partially crashing out. Scanning was from 300nm to 800nm at 0.5nm increments. A 5mL quartz cuvette with four optically polished sides was used to hold our samples. This was due to fluorimeter being next to this spectrophotometer allowing us to use the same prepared sample for both characterizations. System was blanked by scanning our cuvette with the solvent our particles were dispersed in.

3.A.3: Fluorimetry procedure

Fluorimetry was performed on a Shimadzu RF-5301 PC spectrofluorometric fluorometer. A 5mL quartz cuvette optically polished on four sides was used to hold samples during testing. Samples were diluted in solvent before use. Solvents used were tested prior to scanning our samples to ensure they had no emission reading. If a reading was observed from the solvent this would be subsequently subtracted from tested samples data. Samples were scanned at 0.5nm increments at 100 scans per minute. Samples were scanned using an excitation wavelength of 340nm with an observed range of 450nm to 800nm. The data for each sample was transferred individually to an excel file and used to construct a scatter plot of the spectrum

3.A.4: Transmission Electron Microscopy (TEM) imaging procedure

For TEM imaging a JEOL 1400Plus transmission electron microscope was used to observe synthesized particles. Imaging was performed with a voltage setting of 100kv. Images ranged from 100x magnification to 250000x magnification. The filament used was LaB_6. Copper grids (200 mesh) were coated with a thin carbon film and used to hold our

samples during imaging by placing in the sample holder. The copper grids were coated with carbon in lab using carbon-coated mica which was prepared from raw mica and carbon rods. The fixtures which hold the carbon were from Ladd Research Industries: 30170 – carbon rod evaporation unit 30180 - carbon evaporation shield. The carbon was from EMS Cat #70200, sharpened to about 4 mm with a #12040 carbon rod sharpener from E. Fullam. The glass shield was coated with "Bell Shine" from Ladd #30099. Our vacuum evaporator was built by Torr International, model number: TH#-2KW-UPGRD-EB1P operated initially in the 10-6 torr range vacuum range, and at about 40 Amps. The mica was fixed into a clean petri dish which was then placed on a 50mL beaker making it approximately 5-10cm from the graphite rod. The mica was coated using an indirect coating method using a quarter affixed directly above the mica so that the coating would be consistent and reduce the overall thickness of the coat. Water was then used to separate the mica from the carbon by placing water droplets onto a PELCO PTFE immunostaining pad (product #10526-1), purchased from Ted Pella Inc. The carbon-coated mica was cut into small squares, slightly larger than a copper TEM grid, and placed carbon side up into the water droplet at an angle from the side of the droplet to quickly remove the carbon layer. Due to the mica being hydrophilic in nature and carbon being hydrophobic, the mica would sink into the water droplet while the thin layer of carbon would remain at the top of the droplet. The floating carbon film was then lifted onto a copper TEM grid, ensuring that the carbon film covered as much of the grid as possible. The copper grids were washed in hydrochloric acid prior to carbon coating to facilitate breaking through the surface of the droplet. The grid would be placed in a tray to dry by a pair of tweezers. Using a small slip of paper made removing the grid from the tweezers easier as the grid would otherwise stick to the tweezers.

3.A.5: Centrifugation procedure

Centrifugation was performed using an Eppendorf Centrifuge 5415C with a radius of 5.5cm. Samples were centrifuged in 1.7mL GeneMate polypropylene centrifuge tubes from VWR. Samples were centrifuged at 2500rpm for 10 minutes.

3.B: Cadmium sulfide nanoparticle growth

3.B.1: Preparation and handling of [BMIM][$MeSO_4$]

[BMIM][$MeSO_4$] is very hygroscopic. To ensure as pure solvent as possible we used as little [BMIM][$MeSO_4$] at a time as possible. We took our purchased bottle of [BMIM][$MeSO_4$] (1000 mL) to a glove box that had an inert environment and transferred approximately 50mL to a smaller glass bottle that was sealed with a rubber septum. This bottle was stored in a dark drawer. The [BMIM][$MeSO_4$] was transferred under argon with a syringe directly from the bottle, limiting exposure to air/moisture. Before each use it would be sparged with argon to remove as much moisture as possible. Afterwards the septum would be wrapped tightly with parafilm.

3.B.2: Procedure for CdS nanoparticle synthesis

As done previously in section 2.B, we began our experiments with the synthesis of CdS nanoparticles. During this procedure though we would be replacing 1-octadecene and oleic acid with [BMIM][$MeSO_4$] as both our solvent and stabilizing agent. This can be seen in Figure 3.2.

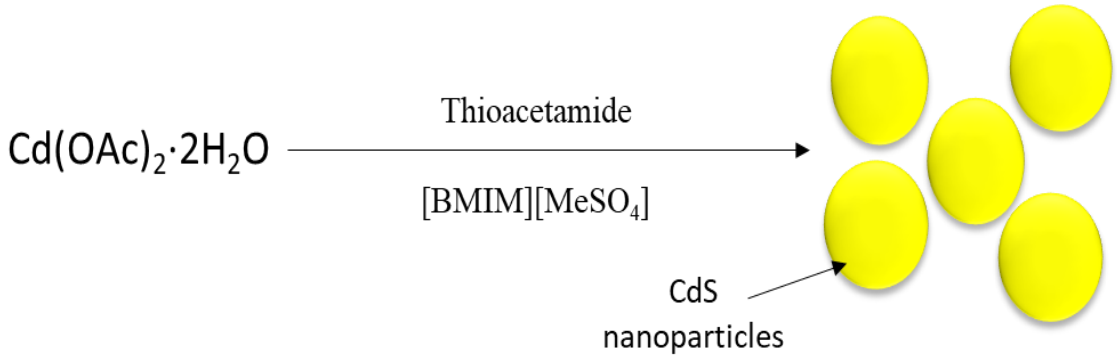

Figure 3.2: Reaction scheme for synthesis of CdS nanoparticles using cadmium acetate dihydrate, thioacetamide, and [BMIM][$MeSO_4$].

A three neck round bottom flask was set up as seen in Figure 3.2. $Cd(OAc)_2 \cdot 2H_2O$ (0.24g, 0.92mmol) and thioacetamide (0.068g, 0.9mmol) were added to the flask which was then sealed with a rubber septum. The air was removed from the flask under vacuum and replaced with argon three times to create an inert environment. 10mL of [BMIM][$MeSO_4$] was transferred via syringe into the flask. The solution was heated to 180°C and held at that temperature for ten minutes during which time the solution began to change to a yellow color.

Once heating was complete the solution was immediately transferred to a sealed 20mL vial at temperature (180°C) with a glass syringe. The solution needed to be moved while still hot due to forming a viscous liquid when cooled that cannot be moved with syringe. Since it was being transferred at high temperatures a glass syringe and all metal needle were used to ensure no rupturing of the syringe or needle during transfer.

At this point, the as-synthesized CdS nanoparticle dispersion can be used directly for the addition of ZnS shells by the SILAR method (described in section 3.C) or the

particles can be purified for characterization (described in the remaining portion of section 3.B below).

In order to characterize our nanoparticles by TEM, they must be removed from the [BMIM][$MeSO_4$]. For characterization, a 1mL aliquot was transferred to a 1.7mL centrifuge tube. The sample was centrifuged at 2500rpm for ten minutes. After centrifugation, a pellet was formed at the bottom of the tube. The supernatant was decanted and the pellet was dispersed in 1mL of DI-H_2O. A TEM grid was prepared as described in materials and preparations section, and the rest of this dispersion was used for UV-vis and fluorimetry.

3.B.3: UV-vis spectroscopy

In preparation for UV-vis spectroscopy approximately 1mL of CdS nanoparticles, dispersed in water, were transferred to a 5mL cuvette with four optically polished windows suitable for both UV-vis and fluorimetry. This was done due to the UV-vis spectrometer and fluorimeter being next to each other and speeding up the process as well as conserving sample. More water was added via pipette to fill the cuvette. The sample was capped and shaken to ensure particles were evenly dispersed within the solution and then UV-vis spectra was obtained using a medium speed with a reading every 0.5nm. A medium speed was chosen to get as accurate a reading while ensuring the particles did not begin to settle. Our UV-vis spectra showed a clear peak is seen at 460nm as seen in Figure 3.3.

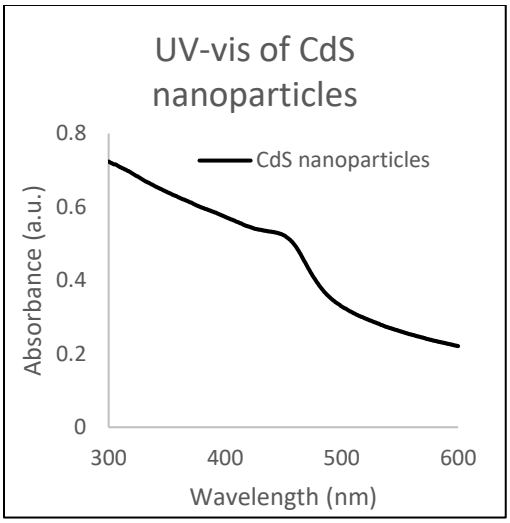

Figure 3.3: The UV-vis spectrum for our CdS nanoparticles in [BMIM][$MeSO_4$] showed an absorbance peak at 460nm.

We attempted to track the growth of the nanoparticles with UV-vis spectroscopy like in section 2.B.4 using samples taken at different points, however the peak remained the same wavelength through all tested time points. This is believed to be because the method used with thioacetamide forms particles much more quickly than the methods we used previously with elemental sulfur.

The CdS nanoparticle synthesis using thioacetamide in [BMIM][$MeSO_4$] involved heating all the reagents together compared to the hot injection method performed using sulfur in 1-octadecene. The one-pot-synthesis with thioacetamide involved all reagents for the synthesis being present from the beginning of the reaction, which allowed for nanoparticles to form as the solution was heated. Once the solution reached the desired temperature of 180°C, the CdS nanoparticles are already formed and reached their maximum size before any samples were taken from the reaction mixture. This growth during heating was further accelerated due to the high reactivity of thioacetamide compared

to elemental sulfur. The hot injection method could be used to prevent this from happening by heating up the cadmium to 180°C before injecting the thioacetamide and allowing the particles to form and grow. In the future an attempt at tracking the growth of the particles in [BMIM][$MeSO_4$] can be done by modifying the experiment to a hot injection method.

3.B.4: TEM imaging

TEM imaging was used to observe the morphology, size, and extent of aggregation of the CdS nanoparticles after being precipitated from [BMIM][$MeSO_4$] and dispersed in water. Roughly spherical particles with average diameter of 4.2nm±0.7nm were observed (Figure 3.4). The majority of particles were not aggregated, though a small number of aggregates were observed. The observation of well-dispersed nanoparticles indicated that irreversible aggregation did not occur in [BMIM][$MeSO_4$] for most of the sample. Aggregates likely formed from the centrifugation process (discussed in section 3.B.6.c).

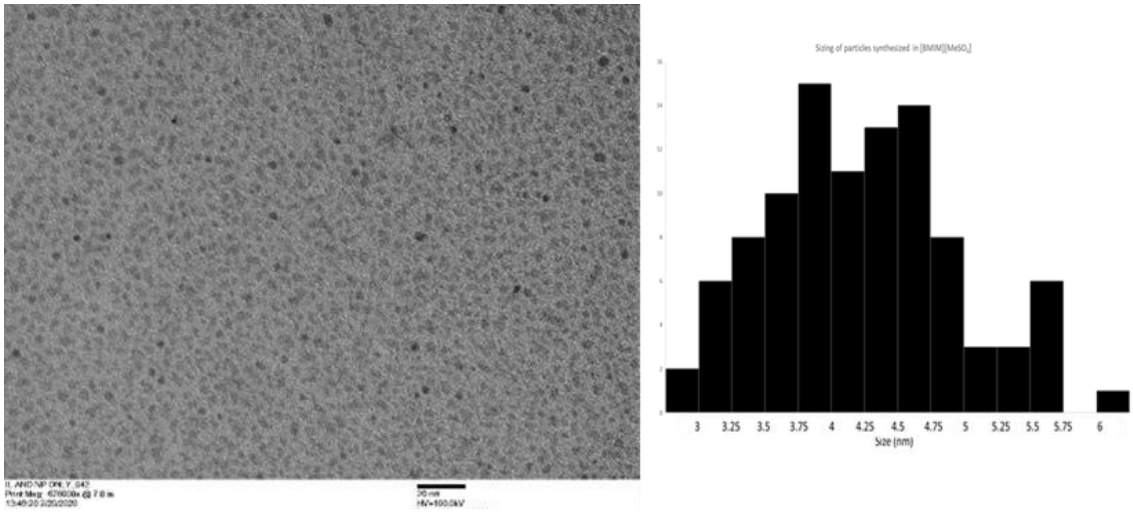

Figure 3.4: TEM imaging and sizing of the CdS nanoparticles dispersed in water after centrifugation. Scale bar equals 20nm. Average diameter was d=4.2nm±0.7nm. 100 particles were sized.

3.B.5: Fluorimetry

The sample was taken directly from the UV-vis spectrometer and inserted into the fluorimeter for scanning. Like the CdS nanoparticles formed in 1-octadecene, the particles synthesized in [BMIM][$MeSO_4$] also have low fluorescence intensity (Figure 3.5). The peak is of low intensity as well as broad. It is also in the same range as the CdS nanoparticles synthesized in 1-octadecene with a peak at around 410nm as seen in Figure 2.15.

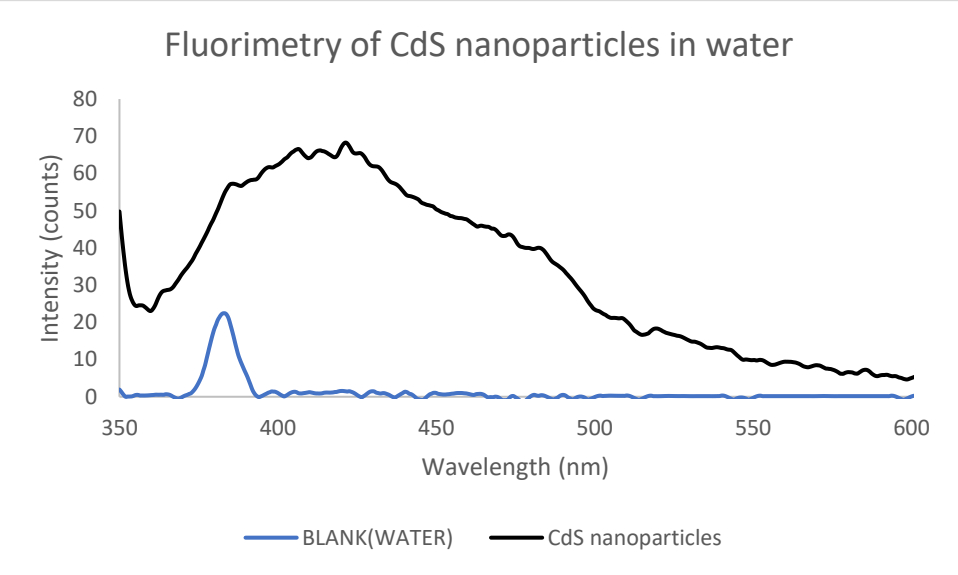

Figure 3.5: Fluorimetry was performed on our purified CdS nanoparticles with an excitation wavelength of 340nm. Like the particles synthesized in 1-octadecene the emission peak is very low.

3.B.6: Issues with synthesis and purification

In order to synthesize our CdS nanoparticles in the [BMIM][$MeSO_4$] we had to undergo many small tests to obtain our new procedure. This pertained to both the reagents chosen, reagents amount, and the purification process and can be seen in Table 3.1.

Table 3.1: Comparing the CdS nanoparticle synthesis in 1-octadecene (from chapter 2) with the CdS nanoparticle synthesis in [BMIM][$MeSO_4$] (chapter 3).

	Synthesis in 1-octadecene (chapter 2)	**Synthesis in [BMIM][$MeSO_4$] (chapter 3)**
Method	Hot injection	One-pot-synthesis
Cadmium reagent	$Cd(OAc)_2 \cdot 2H_2O$	$Cd(OAc)_2 \cdot 2H_2O$
Sulfur reagent	Elemental sulfur	Thioacetamide
Solvent	1-Octadecene & oleic acid	[BMIM][$MeSO_4$]
Temperature synthesized	260°C	180°C
Preparation for optical spectroscopy	None	Precipitated and dispersed in water
Preparation for TEM imaging	Precipitated and dispersed in hexanes	Precipitated and dispersed in water

3.B.6.a: Issues with [BMIM][$MeSO_4$]

As stated earlier, [BMIM][$MeSO_4$] had to be used carefully due to being hygroscopic. Another issue observed occurred when heating the [BMIM][$MeSO_4$] to dissolve the $Cd(OAc)_2 \cdot 2H_2O$. When the [BMIM][$MeSO_4$] was heated to over 200°C it would begin to change color from a brown color to black. This color change at about 200°C would be a slow change taking over an hour to fully change to black. At over 260°C this color change would occur by the time the solution reached temperature. This color change also occurred more quickly with sulfur and thioacetamide, changing to a transparent black solution on a hot plate temperature of 190°C. This made it difficult to tell when the cadmium was fully dissolved as we could no longer rely on color change. Heating also

caused a change once the [BMIM][$MeSO_4$] was cooled, as it would change into a viscous liquid. As we discovered previously, $Cd(OAc)_2 \cdot 2H_2O$ dissolved at 180°C, therefore we lowered the temperature so the [BMIM][$MeSO_4$] would not change properties.

A second issue with [BMIM][$MeSO_4$] is that it is non-volatile, meaning it will never evaporate. Due to this we could not cast grids with our crude product with no purification.

A third issue with [BMIM][$MeSO_4$] was that it had a UV-vis reading due to scattering, and we could not observe a peak from CdS nanoparticles in our crude product directly. Therefore, purification was needed not just for TEM imaging but also for UV-vis and fluorimetry. As Figure 3.6 shows, [BMIM][$MeSO_4$] after being heated has an absorbance reading through the entire range that our CdS nanoparticle absorbance peaks can appear.

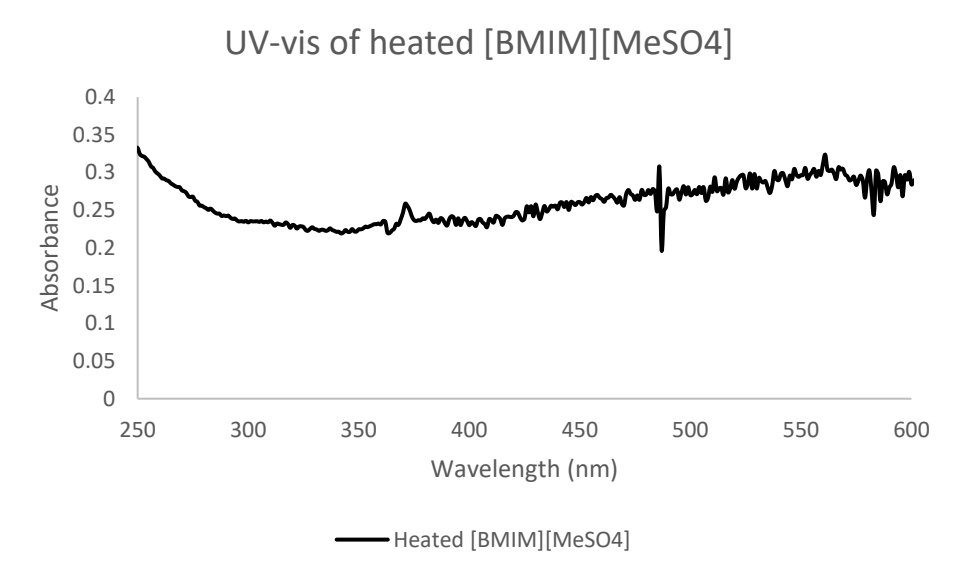

Figure 3.6: [BMIM][$MeSO_4$] seemed to cause scattering under UV-vis, preventing us from performing UV-vis on our crude product. This meant that we had to perform purification for UV-vis spectroscopy on our particles

3.B.6.b: Issues with CdS nanoparticle synthesis

Our first attempt at CdS nanoparticle synthesis involved following the procedure from 2.B but using [BMIM][$MeSO_4$] as our solvent and stabilizing agent instead of 1-octadecene and oleic acid. This procedure yielded inconclusive UV-vis data. While only a small number, TEM imaging showed that we had synthesized nanoparticles. We increased the concentration of $Cd(OAc)_2 \cdot 2H_2O$ and sulfur powder by five times in order to synthesize more particles. This also yielded inconclusive UV-vis data. TEM imaging showed a minor increase in the number of particles, however these particles were aggregated. We switched our sulfur source from elemental sulfur to thioacetamide due to its higher reactivity as well as previous studies using thioacetamide to synthesize nanoparticles in [BMIM][$MeSO_4$].[22] TEM imaging of these CdS nanoparticles synthesized with thioacetamide showed a substantial increase in the amount of particles. With a method that yielded a high number of particles we could focus on optimizing the purification process to obtain UV-vis data.

3.B.6.c: Issues with purification process

Purification was needed in order to remove our particles from the [BMIM][$MeSO_4$]. Even trace amounts of [BMIM][$MeSO_4$] could form an organic layer that the TEM electron beam could not pierce. As seen in Figure 3.7, a thick film of organic material from the [BMIM][$MeSO_4$] prevents the nanoparticles from being seen. The electron beam cannot pierce the film of organics, only searing a partial hole where the beam is condensed.

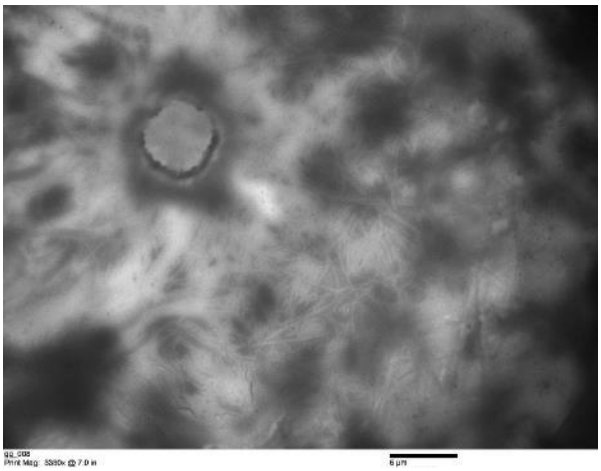

Figure 3.7: TEM image of a CdS nanoparticle dispersion in hexane/oleic acid with residual [BMIM][$MeSO_4$] preventing detection of particles.

While centrifugation was ultimately the method of purification we chose to remove the [BMIM][$MeSO_4$], it took many steps to reach an optimized procedure. While these steps were in themselves unsuccessful, each one provided a small piece of information that allowed us to improve our purification process to finally be able to obtain UV-vis data.

Our initial purification process was liquid-liquid extraction. While ultimately unsuccessful, it did prove to us we were forming nanoparticles. This method was done by using [BMIM][$MeSO_4$] and an immiscible solvent containing dissolved oleic acid as a ligand. Our first study was to determine which solvents would allow us to form two phases with [BMIM][$MeSO_4$]. We tested acetone, toluene, hexanes, and tetrahydrofuran (THF) and found that hexanes and toluene were both immiscible with the neat ionic liquid, while acetone formed a second phase when oleic acid was added to [BMIM][$MeSO_4$]. THF was not studied further. Figure 3.8 shows the process for our liquid-liquid extraction. We took 1mL of our crude product in 2mL vial and added 1mL of an organic solvent mixed with oleic acid at different concentrations. These vials were then shaken/vortexed to attempt and

pull the CdS particles from the [BMIM][$MeSO_4$] into the organic solvent/oleic acid mixture. These extractions never gave us UV-vis data showing we had synthesized particles; however, they did provide useful TEM images as seen in Figure 3.9. These TEM images showed that we had synthesized nanoparticles, but this purification procedure was not useful for obtaining UV-vis or fluorimetry spectra.

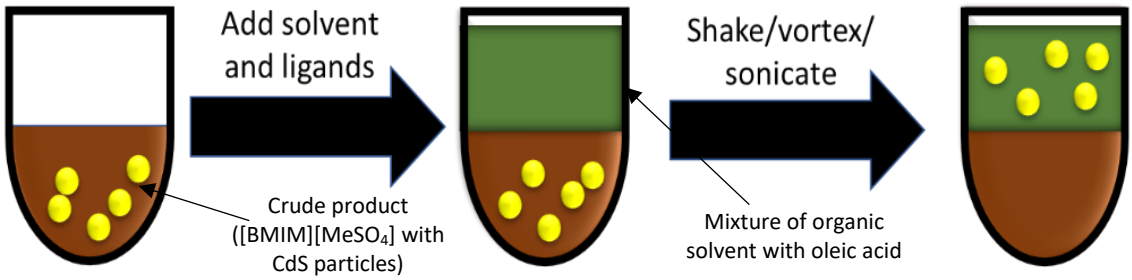

Figure 3.8: Scheme showing liquid-liquid extraction experiments using oleic acid with an organic solvent (hexanes, toluene, or acetone). The mixtures had ratios of 2:1 organic solvent:oleic acid, as well as 20:1, 50:1, and 100:1.

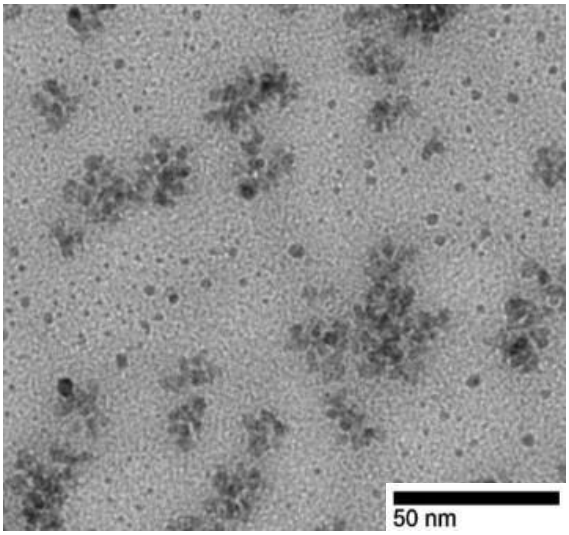

Figure 3.9: TEM image from a liquid-liquid extraction using 20:1 toluene:oleic acid showing a few free particles, most though are aggregated together. The scale bar represents 50 nm.

Since liquid-liquid extractions were not working our next attempt was centrifugation to separate our particles from the [BMIM][$MeSO_4$]. This procedure is illustrated in Figure 3.10. To determine the best solvent for the crashed out CdS particles, we centrifuged four 1mL samples of crude product at 6000 rpm for 10 minutes to obtain a pellet in each centrifuge tube. Acetone, isopropanol, THF, and water were then used as solvents to try and disperse the particles. Of these, only water fully dispersed the particles and formed one phase. Particles dispersed in water were found to have the fewest aggregates (Figure 3.11). We also observed web-like structures in the TEM images of this water dispersion, but these structures were not reproducible.

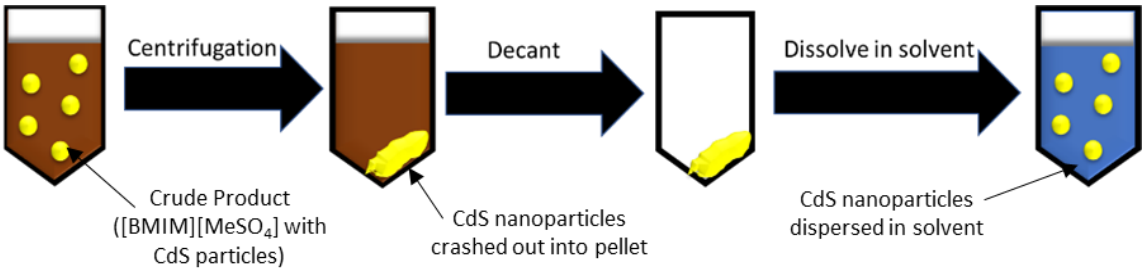

Figure 3.10: Scheme for centrifugation experiments.

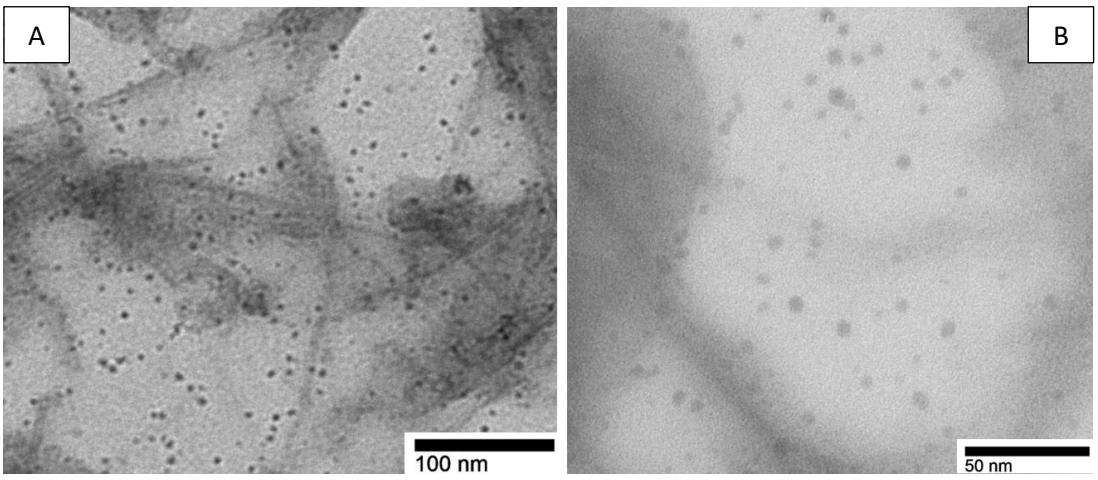

Figure 3.11: TEM images obtained from CdS nanoparticles dispersed in water. The right image is a magnified region of the left image to show individual particles.

Once we had determined the best solvent to disperse our particles in after centrifugation we decided to optimize our precipitation procedure. We first wanted to determine the optimal number of centrifugations we could perform. More centrifuges would allow us to obtain a purer product. Therefore, 1mL of crude product with CdS nanoparticles were added to two centrifuge tubes. Each was centrifuged at 6000rpm for ten minutes. Both had the supernatant decanted. One sample was dispersed in water and a TEM sample was prepared (Figure 3.12a). The second sample was dispersed in 1mL of isopropanol, centrifuged at 6000rpm for ten minutes to obtain a white pellet. The supernatant was decanted and the pellet was dispersed in isopropanol and precipitated by centrifugation once more. The supernatant was decanted and the pellet dispersed in water and a sample prepared for TEM imaging (Figure 3.12b). As Figure 3.12 shows, after more than one centrifuge, our particles form large aggregates with no free particles. However, even the sample obtained after one centrifugation procedure did not give a clean UV-vis peak. We attributed these inconclusive UV-vis spectra to either multiple size particles crashing out together, thus broadening the peak due to their different absorbance peaks, or from more [BMIM][$MeSO_4$] being crashed out with the particles thus distorting the spectrum.

Since we could not improve our method via number of centrifuges, we decided to optimize centrifuge speed. All previous attempts had spin speeds at 6000rpm for ten minutes. For this study we decided to try and find the lowest possible centrifuge speed that would obtain a pellet. We decided to try and obtain the particles that were all the same size, and by centrifuging at the lowest possible speed the larger particles would preferentially

crash out. This led to us lowering the centrifugation speed from 6000rpm to 2500rpm which gave us our first absorbance peak for our particles synthesized in [BMIM][$MeSO_4$] which can be seen in Figure 3.3.

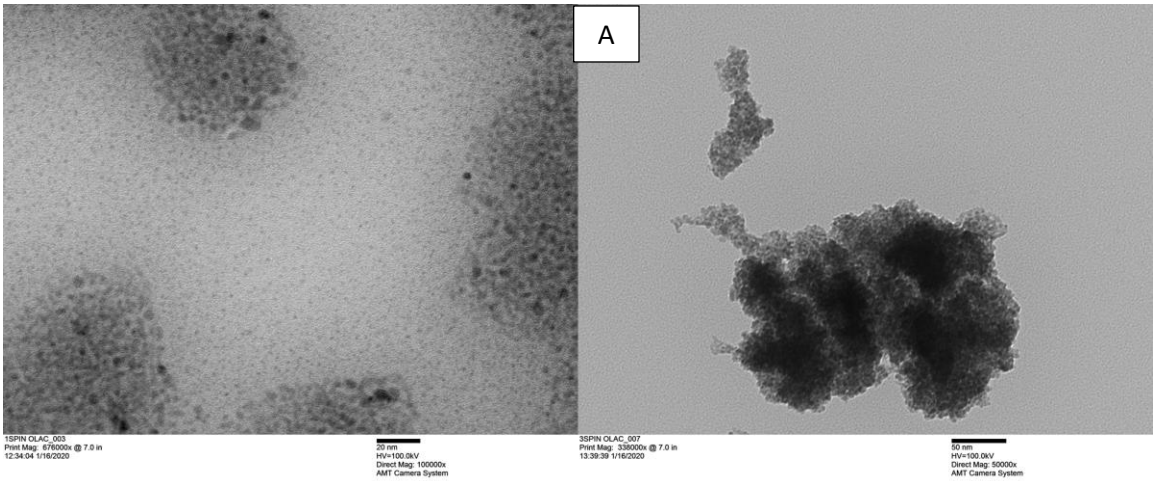

Figure 3.12: TEM images obtained after centrifugation at 6000 rpm once (a) and three times (b). Image-A scale bar=20nm. Image-B scale bar=50nm

3.C: Planned future experiments: zinc sulfide shell growth

3.C.1: Procedure for ZnS shell growth

CdS nanoparticles would be synthesized following the procedure from section 3.B.2. However, a three-way distillation head will be attached to the flask. The water jacket condenser will be attached to the side of the distillation head, leading to a beaker. This will allow moisture to leave the reaction vessel. A solution will be made by adding thioacetamide (0.272g, 3.61mmol) to a 20mL vial. The vial will be sealed with rubber septum and atmosphere will be vacuumed out and replaced with argon. Then 5mL of [BMIM][$MeSO_4$] will be added to vial via syringe under argon. The solution will be heated on hot plate set to 100°C to dissolve thioacetamide. A zinc solution will be made by adding

$Zn(OAc)_2 \cdot 2H_2O$ (0.806g, 3.61mmol) to 20mL vial. This will then be dissolved in as little DI-H_2O as possible at room temperature. The amount of water needed to fully dissolve the $Zn(OAc)_2 \cdot 2H_2O$ will be determined in lab. Vial is shaken and vortexed until $Zn(OAc)_2 \cdot 2H_2O$ is dissolved.

After CdS nanoparticles are synthesized a 0.7mL sample will be transferred to 2mL vial. 0.65mL of the thioacetamide solution will be transferred to flask via syringe and allowed to sit at 180°C for five minutes. An equivalent amount of zinc acetate dihydrate will be added to flask as an aqueous solution via syringe and allowed to sit for five minutes, after which a 0.7mL sample will be transferred to a 2mL flask. This procedure will be repeated with increasing amounts of sulfur and zinc added to grow subsequent shells as seen in Table 3.2 and 0.7mL samples will be transferred to 2mL vials for purification and characterization. Purification will follow same procedure from 3.B.2.

Table 3.2: Estimated amounts of $Zn(OAc)_2 \cdot 2H_2O$ and thioacetamide needed to grow six ZnS layers on CdS nanoparticles.

Shell number	Amount in mmol
1	0.47
2	0.59
3	0.72
4	0.87
5	1.0
6	1.2

3.C.2: Calculating amounts of zinc and thioacetamide needed to grow multiple ZnS layers

Due to the large number of particles synthesized using thioacetamide samples must be heavily diluted in order to obtain UV-vis data. Calculations for the amounts of sulfur and zinc needed for each layer are estimated using stoichiometry instead of absorbance peak from UV-vis. For our estimations we assumed that $Cd(OAc)_2 \cdot 2H_2O$ and thioacetamide fully reacted during CdS nanoparticle synthesis. Size determination of particles was obtained from TEM imaging. As stated in section 3.B.2, CdS nanoparticles are fully grown when synthesized with thioacetamide by the time they reach 180°C. Therefore, we can assume the size of the particles will be approximately the same during each synthesis. After sizing our CdS particles we determined their approximate size to be 5nm in diameter (2.5nm radius). This can then be converted into volume (using $4\pi r^3$) then into mass by multiplying the volume by the density of CdS ($4.8 g/cm^3$). The moles of CdS per particle can be estimated by dividing the mass per particle by molar mass of CdS (144.47g/mol). By assuming all our $Cd(OAc)_2 \cdot 2H_2O$ reacted, we can divide the starting number of $Cd(OAc)_2 \cdot 2H_2O$ moles (0.9mmol) by the moles of CdS per particle to determine the number of CdS nanoparticles in solution. The radius of the CdS/ZnS core/shell particle can be estimated by adding 0.31nm to the radius of the CdS. Volume can then be calculated (using $4\pi r^3$). The volume of the ZnS shell can then be estimated by subtracting the CdS nanoparticle volume from the CdS/ZnS core/shell particle as shown in Figure 2.9. The mass of the ZnS shell can be estimated by multiplying the estimated volume of the ZnS shell with the density of ZnS ($4.09 g/cm^3$). Moles of ZnS per shell is estimated by dividing the mass per ZnS shell by the molar mass of ZnS (97.47g/mol). The moles of ZnS per shell

can then be multiplied by the number of CdS nanoparticles in solution to determine the moles of thioacetamide and $Zn(OAc)_2 \cdot 2H_2O$ needed to coat all particles. This process can be repeated with all the same numbers except for the radius of the next layered particle, which will have a radius 0.31nm longer than the last particle.

Chapter 4: Conclusion

We were able to successfully synthesize CdS/ZnS core/shell nanoparticles in 1-octadecene with insulating ligands attached. We were able to determine what size nanoparticles we wished to synthesize. Characterization was performed to prove we had characterized the correct size particles as well as the correct composition. With this we could use these particles as a basis for comparison for subsequent experiments.

CdS nanoparticles were also successfully synthesized using [BMIM][$MeSO_4$] as a solvent and stabilizing agent. These particles were successfully extracted and characterized using UV-vis, fluorimetry, and TEM imaging. Purification process for extracting the particles was optimized to allow particles to be characterized. Addition of a ZnS shell for the synthesis of CdS/ZnS core/shell nanoparticles in [BMIM][$MeSO_4$] has not yet been successfully performed. Calculations for estimates on the amount of zinc and sulfur needed for shell growth have been created along with a procedure for future attempts at shell growth.

References

(1) Frequently Asked Questions (FAQs) - U.S. Energy Information Administration (EIA) https://www.eia.gov/tools/faqs/faq.php (accessed Jul 5, 2020).

(2) McMullan, J. T. Energy, the Solar-Hydrogen Alternative, J. O'm. Bockris, Architectural Press, London, 1976. Price: £13.50. No. of Pages: 365, Isbn 0 85139 J83 X. *International Journal of Energy Research* **1977**, *1*, 369–369.

(3) Koppel, T. Hawaii: RE in the Island State. *Refocus* **2001**, *2*, 10–13.

(4) Fujishima, A.; Honda, K. Electrochemical Photolysis of Water at a Semiconductor Electrode. *Nature* **1972**, *238*, 37–38.

(5) Zou, H.; Dong, C.; Li, S.; Im, C.; Jin, M.; Yao, S.; Cui, T.; Tian, W.; Liu, Y.; Zhang, H. Effect of Surface Trap States on Photocatalytic Activity of Semiconductor Quantum Dots. *The Journal of Physical Chemistry C* **2018**, *122*, 9312–9319.

(6) Wu, K.; Chen, Z.; Lv, H.; Zhu, H.; Hill, C. L.; Lian, T. Hole Removal Rate Limits Photodriven H2 Generation Efficiency in CdS-Pt and CdSe/CdS-Pt Semiconductor Nanorod–Metal Tip Heterostructures. *Journal of the American Chemical Society* **2014**, *136*, 7708–7716.

(7) Jiang, D.; Sun, Z.; Jia, H.; Lu, D.; Du, P. A Cocatalyst-Free CdS Nanorod/ZnS Nanoparticle Composite for High-Performance Visible-Light-Driven Hydrogen Production from Water. *Journal of Materials Chemistry A* **2016**, *4*, 675–683.

(8) Hayes, R.; Warr, G. G.; Atkin, R. Structure and Nanostructure in Ionic Liquids. *Chemical Reviews* **2015**, *115*, 6357–6426.

(9) Mai, N.-L.; Ahn, K.; Koo, Y.-M. Methods for Recovery of Ionic Liquids—A Review. *Process Biochemistry* **2014**, *49*, 872–881.

(10) Welton, T. Room-Temperature Ionic Liquids. Solvents for Synthesis and Catalysis. *Chemical Reviews* **1999**, *99*, 2071–2084.

(11) Neouze, M.-A. About the Interactions between Nanoparticles and Imidazolium Moieties: Emergence of Original Hybrid Materials. *Journal of Materials Chemistry* **2010**, *20*, 9593–9607.

(12) Almeida, H. F. D.; Carvalho, P. J.; Kurnia, K. A.; Lopes-da-Silva, J. A.; Coutinho, J. A. P.; Freire, M. G. Surface Tensions of Ionic Liquids: Non-Regular Trend Along the Number of Cyano Groups. *Fluid phase equilibria* **2016**, *409*, 458–465.

(13) Weingärtner, H. Understanding Ionic Liquids at the Molecular Level: Facts, Problems, and Controversies. *Angewandte Chemie International Edition* **2008**, *47*, 654–670.

(14) Janiak, C. Ionic Liquids for the Synthesis and Stabilization of Metal Nanoparticles. *Zeitschrift für Naturforschung B* **2013**, *68*, 1059–1089.

(15) Ravishankar, T. N.; Vaz, M. de O.; Khan, S.; Ramakrishnappa, T.; Teixeira, S. R.; Balakrishna, G. R.; Nagaraju, G.; Dupont, J. Enhanced Photocatalytic Hydrogen Production from Y2O3/TiO2 Nano-Composites: A Comparative Study on Hydrothermal Synthesis with and without an Ionic Liquid. *New Journal of Chemistry* **2016**, *40*, 3578–3587.

(16) Yu, W. W.; Qu, L.; Guo, W.; Peng, X. Experimental Determination of the Extinction Coefficient of CdTe, CdSe, and CdS Nanocrystals. *Chemistry of Materials* **2003**, *15*, 2854–2860.
(17) Schneider, C. A.; Rasband, W. S.; Eliceiri, K. W. NIH Image to ImageJ: 25 Years of Image Analysis. *Nature Methods* **2012**, *9*, 671–675.
(18) Jia, X.; Huang, L.; Gao, R.; Devaraji, P.; Chen, W.; Li, X.; Mao, L. Improvement of Photocatalytic Hydrogen Generation of Leaves-like CdS Microcrystals with a Surface Decorated by Dealloyed Pt-Co Nanoparticles. *Solar Energy* **2020**, *206*, 8–17.
(19) Chen, D.; Zhao, F.; Qi, H.; Rutherford, M.; Peng, X. Bright and Stable Purple/Blue Emitting CdS/ZnS Core/Shell Nanocrystals Grown by Thermal Cycling Using a Single-Source Precursor. *Chemistry of Materials* **2010**, *22*, 1437–1444.
(20) Peng, X.; Schlamp, M. C.; Kadavanich, A. V.; Alivisatos, A. P. Epitaxial Growth of Highly Luminescent CdSe/CdS Core/Shell Nanocrystals with Photostability and Electronic Accessibility. *Journal of the American Chemical Society* **1997**, *119*, 7019–7029.
(21) Veamatahau, A.; Jiang, B.; Seifert, T.; Makuta, S.; Latham, K.; Kanehara, M.; Teranishi, T.; Tachibana, Y. Origin of Surface Trap States in CdS Quantum Dots: Relationship between Size Dependent Photoluminescence and Sulfur Vacancy Trap States. *Physical Chemistry Chemical Physics* **2015**, *17*, 2850–2858.
(22) Biswas, K.; Rao, C. N. R. Use of Ionic Liquids in the Synthesis of Nanocrystals and Nanorods of Semiconducting Metal Chalcogenides. *Chemistry - A European Journal* **2007**, *13*, 6123–6129.